Bull Volcanol (2004) 66:541–561
DOI 10.1007/s00445-004-0340-3

RESEARCH ARTICLE

Marie-Christine Gerbe · Jean-Claude Thouret

Role of magma mixing in the petrogenesis of tephra erupted during the 1990–98 explosive activity of Nevado Sabancaya, southern Peru

Received: 29 January 2003 / Accepted: 27 November 2003 / Published online: 12 March 2004

Abstract The Nevado Sabancaya in southern Peru has exhibited a persistent eruptive activity over eight years following a violent eruption in May–June 1990. The explosive activity consisted of alternated vulcanian and phreatomagmatic events, followed by declining phreatic activity since late 1997. The mean production rate of magma has remained low (10^6–10^7 m^3 per year).

The 1990–1998 eruptive episode produced andesitic and dacitic magmas. The juvenile tephra span a narrow range of compositions (60–64 wt% SiO_2). While SiO_2 contents do vary slightly, they do not show any systematic variation with time. Phenocryst assemblages in the juvenile rocks consist of mainly plagioclase, associated with high-Ca pyroxene, hornblende, biotite, and iron-titanium oxides. Rare fine-grained magmatic enclaves, with angular to subrounded shapes, are contained within some of the juvenile lava blocks, which were expelled since 1992. They have a homogeneous andesitic composition (57 wt% SiO_2) and show randomly oriented interlocking columnar or acicular crystals (plagioclase and amphibole), with interstitial glass and a few voids, which define a quench-textured groundmass.

Textural, mineralogical and chemical evidence suggests that the 1990–1998 eruptions have mainly erupted hybrid andesites, except for the 1990 dacite. The hybrid andesites contain a mixed population of plagioclase phenocrysts: Ca-rich clear plagioclase ($An_{40–60}$), Na-rich clear plagioclase ($An_{25–35}$), and inversely zoned "dusty-rimmed" plagioclase with a sodic core ($An_{25–40}$) surrounded by a Ca-rich mantle ($An_{45–65}$). Melt-inclusions, wavy dissolution surfaces and stepped zoning within the "dusty-rimmed" plagioclases are compatible with resorption induced by magma recharge events. Chemical and isotopic lines of evidence also show that andesites are hybrids resulting from magma mixing processes. Repeated magma recharge, incomplete homogenisation and different degrees of crustal assimilation may explain the extended range of isotopic signatures.

Our study leads to propose an evolution model for the magmatic system at Nevado Sabancaya. The main magma body consisted of dacitic magmas differentiating through extensive open-system crystallization (AFC). Repeated recharge of more mafic magmas induced magma mixing, leading to the formation of hybrid andesites. A partially crystalline boundary layer formed at the interface between the andesites and the recharge magma. The magmatic enclaves were produced by the disruption and dispersion of this andesitic layer as a result of new magma injection and/or sustained tectonic activity.

Periodic magma recharge and interactions with groundwater are two processes that have enabled the explosive regime to remain persistent over an 8-year-long period. What precise mechanism triggers the eruptive activity remains speculative, but it may be related either to new magma injection, or to the sustained tectonic activity that occurred at that time in the vicinity of the volcano, or a combination of both.

Keywords Nevado Sabancaya · Peru · Magmatic enclaves · Magma mixing · Andesite · Dacite · Explosive activity

M.-C. Gerbe (✉)
Département de Géologie-Pétrologie-Géochimie,
UMR 6524 CNRS "Magmas et Volcans", Université Jean Monnet,
23 rue du Dr. Paul Michelon, 42023 Saint Etienne cedex 2, France
e-mail: gerbe@univ-st-etienne.fr
Fax: +33-4-77485108

J.-C. Thouret
Laboratoire Magmas et Volcans, OPGC,
Université Blaise Pascal et CNRS,
5 rue Kessler, 63038 Clermont-Ferrand cedex, France

Introduction

Long-lived explosive regimes, which occur on some calc-alkaline arc volcanoes, remain poorly explained, since they generally correspond to rather small volumes of ejected products related to low magma supply rates. Nevado Sabancaya (15°47′S, 71°51′W) in southern Peru (Fig. 1a) has shown such a persistent explosive activity over eight years following a violent eruption in May-June

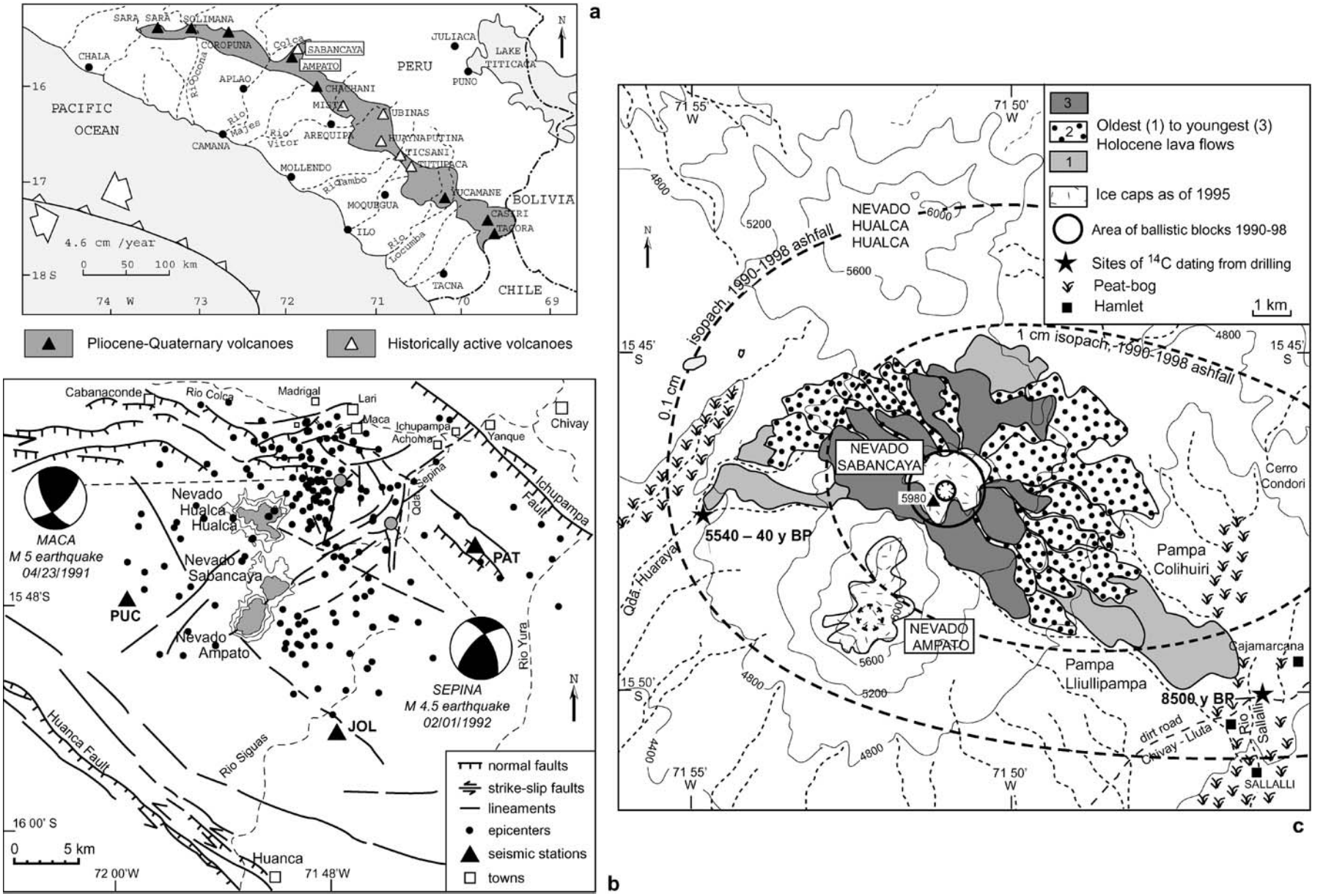
a
SARA SARA
SOLIMANA
COROPUNA
Colca
SABANCAYA
AMPATO
CHALA
Rio Ocoña
APLAO
CHACHANI
MISTI
UBINAS
PERU
JULIACA
LAKE TITICACA
PUNO
PACIFIC OCEAN
Rio Majes
Rio Vitor
AREQUIPA
HUAYNAPUTINA
TICSANI
CAMANA
MOLLENDO
Rio Tambo
UTUTIPACA
YUCAMANE
BOLIVIA
MOQUEGUA
CASIRI
TACORA
ILO
Rio Locumba
4.6 cm /year
0 50 100 km
TACNA
CHILE
16
17
18 S
74 W
73
72
71
70
69
N
Pliocene-Quaternary volcanoes
Historically active volcanoes
b
Cabanaconde
Rio Colca
Madrigal
Lari
Maca
Ichupampa
Achoma
Yanque
Chivay
Qda. Sepina
Ichupampa Fault
Nevado Hualca Hualca
MACA
M 5 earthquake
04/23/1991
Nevado Sabancaya
PAT
15 48'S
PUC
Nevado Ampato
SEPINA
M 4.5 earthquake
02/01/1992
Rio Yura
N
JOL
Huanca Fault
Rio Siguas
normal faults
strike-slip faults
lineaments
epicenters
seismic stations
towns
16 00' S
0 5 km
72 00'W
Huanca
71 48'W
c
71 55' W
71 50' W
NEVADO HUALCA HUALCA
6000
5200
5600
4800
N
isopach, 1990-1998 ashfall
0.1 cm
1 cm isopach, 1990-1998 ashfall
15 45' S
NEVADO SABANCAYA
5980
5540 – 40 y BP
Qda. Huaraya
Cerro Condori
Pampa Colihuiri
NEVADO AMPATO
6000
15 50' S
Pampa Lliullipampa
Cajamarcana
8500 y BP
dirt road
Chivay - Lluta
Rio Sallalli
SALLALLI
4400
3
2
1
Oldest (1) to youngest (3) Holocene lava flows
Ice caps as of 1995
Area of ballistic blocks 1990-98
Sites of 14C dating from drilling
Peat-bog
Hamlet
1 km

1990. The eruptive activity consisted of alternated vulcanian and phreatomagmatic events which produced small volumes of tephra and have varied through time in intensity and frequency.

Certain active volcanoes from subduction zones around the world exhibit long-lived vulcanian activity interrupted by major crises. Sakura-jima, Japan, and Semeru, Java, are quite remarkable for their continuous, mainly vulcanian, explosive activity, which has continued for more than 40 years. Galeras, Colombia, also experienced continuous eruptive activity since 1989, including several major vulcanian events during the five first years. At Galeras, intense gas pressurisation within the magmatic system was responsible for triggering eruptions and was induced by the previous emplacement of a lava dome (Stix et al. 1997). Subsequent cyclic pressurisation has been proposed to explain the persistent vulcanian activity. Such a model of vulcanian activity is unable to explain activity at Nevado Sabancaya. There is no evidence of the emplacement of a lava dome or magma plug in the conduit prior to eruption, and furthermore intense fumarolic activity suggests continuous degassing.

The 1990–1998 eruption has produced andesitic to dacitic juvenile tephra, some of which contain mafic magmatic enclaves. In this study, the term "magmatic enclave" is preferred to "magmatic inclusion", following the nomenclature proposed by Didier and Barbarin (1991). Magmatic enclaves are commonly related to the mingling of coexisting magmas with strongly contrasting physical properties (Bacon 1986), and to periodic recharge of more mafic magmas. Influx of magma into the reservoir is a mechanism which triggers eruptions because it corresponds to major thermal and mechanical disruption (Sparks et al. 1977; Eichelberger 1980; Murphy et al. 1998).

The scope of this paper is to document the petrography, mineralogy and geochemistry of the juvenile tephra and their magmatic enclaves erupted during the 1990–1998 eruptions at Nevado Sabancaya. Available volcanic, seismic and tectonic data are compared to and integrated with the petrological and geochemical data. The ultimate goals are to define and characterise the petrogenetic processes leading to the genesis and evolution of magmas, to evaluate the pre-eruptive magmatic conditions, to examine the possible triggering mechanisms for eruptions, and to understand how and why the unrest lasted eight years.

Regional geologic setting and eruptive history of Nevado Sabancaya

Nevado Sabancaya, located within the Western Cordillera in the central Andean volcanic zone (CVZ), belongs to the group of six active volcanoes in southern Peru (Fig. 1a). The Western Cordillera in southern Peru consists of Mesozoic and Cenozoic sedimentary and volcanic formations unconformably overlying a Precambrian basement (Kink et al. 1986; Mégard 1987; Palacios 1995). During the Cenozoic, continental volcanic rocks and volcaniclastic sediments were deposited discontinuously, punctuated by discrete compressive tectonic phases which were coeval with periods of high convergence rate of the lithospheric plates (Sébrier et al. 1988; Sébrier and Soler 1991). Tensional faulting prevailed in the Western Cordillera and was associated with voluminous calc-alkaline volcanism (Kanokea and Guevara 1984; Soler 1990; Sébrier and Soler 1991). Large volumes of lavas, ignimbrites and volcaniclastic sediments were deposited, forming the Neogene basement of the huge Plio-Quaternary composite volcanoes.

Three trends of active faults are identified in the Nevado Sabancaya region (Fig. 1b). (i) Two N135-striking fault zones, the Ichupampa and Huanca, are mainly characterised by dip-slip motions with a small sinistral strike-slip component (Mering et al. 1996; Antayhua 2001). They form regional scale extensional lineaments, parallel to the trench, which affect the whole Arequipa region in southern Peru (Fig. 9 in Huaman et al. 1993; Mering et al. 1996). (ii) A N85-trending fault system, located at the southern edge of the Rio Colca valley (Fig. 1b), also represents a major trend on a regional scale and is mainly characterised by southward dip-slip motions. The N135 and N85 fault systems comprise the major Holocene tectonic activity (Sébrier et al. 1985; Antayhua 2001). (iii) Auxiliary N50-trending faults, which also show dip-slip motions, are present as well (Fig. 1b). These extensional fractures, although of local extent, appear to be directly related to the Quaternary volcanoes. The eruptive centres of Nevado Ampato and Nevado Sabancaya sit astride a zone of N50-trending lineaments that roughly parallel the NNE-SSW oriented Qda. Sepina valley (Fig. 1b). In 1991 and 1992, two high-magnitude earthquakes (5 and 4.5, respectively) were located in the Rio Colca and the Qda. Sepina valleys about 10 km NNE of Nevado Sabancaya (Fig. 1b). These shallow tectonic earthquakes, related to N50-fault motions, had hypocentres located at a depth of about 24 km (Antayhua 2001). Numerous tectonic earthquakes of low-

Fig. 1a–c **a** Location map of Nevado Sabancaya within southern Peru (CVZ). **b** Tectonic map of the Nevado Sabancaya-Rio Colca area and spatial distribution of the epicentres of earthquakes recorded during 1993–95 (Mering et al. 1996; Antayhua et al. 2001). Focal mechanisms of two high-magnitude earthquakes are also shown (Antayhua 2001). A seismic telemetry network, composed of 3 short-period seismometers (solid triangles) recorded numerous tectonic earthquakes with ML magnitude <3.0 and maximum depth of 24 km, which were concentrated in the Pampa Sepina area about 10 km N-NE of the volcano. From 1992 to 1996, surface inflation was also recorded in the same area (Prittchard and Simons 2002). Abbreviations for seismic stations are: *PUC* = Pucarillo, *JOL* = Jolla Jello, *PAT* = Patapampa. **c** Sketch map of Nevados Sabancaya and Ampato, showing the Holocene lava field of Nevado Sabancaya. Geomorphological criteria distinguish three generations of block-lava flows (modified after Huaman et al. 1993 and Thouret et al. 1994). Their Holocene age is confirmed by ^{14}C dating of organic matter trapped below a lava flow from the older generation (Thouret et al. 2001). The cumulative thickness and extent of the 1990–1998 ashfall deposit is also reported

er magnitude also occurred during the eruptive crisis (Fig. 1b). Their epicentres were mainly concentrated in the area of the Pampa Sepina, about 10–15 km NNE of Nevado Sabancaya (Antayhua et al. 2001).

Nevado Sabancaya is the youngest volcano of a massif consisting of three centres: Nevado Hualca Hualca to the north, Nevado Sabancaya and Nevado Ampato to the south (Fig. 1b). They stand on a plateau consisting of Neogene volcanic rocks (de Silva and Francis 1991; Thouret et al. 1994). A dacitic ignimbrite from an upper unit on the plateau gives an age of 2.2±0.15 Ma ($^{40}Ar/^{39}Ar$ on plagioclase phenocrysts, "Laboratoire Magmas et Volcans", Université Blaise Pascal, France). Consequently, the Nevado Hualca Hualca, the oldest stratovolcano, was probably constructed during the late Pliocene and early Pleistocene. The Nevado Sabancaya and Nevado Ampato form a less dissected massif, consisting of a series of lava domes aligned along a N50 trend, decreasing in age from SW to NE and associated with block lava flows (Fig. 1c). The morphology of these volcanoes, slightly affected by glacial erosion, suggests a more recent growth than Nevado Hualca Hualca. An andesitic lava flow emplaced over the Pliocene ignimbrites and forming the basement of the two stratovolcanoes gives an age of 0.80±0.04 Ma ($^{40}Ar/^{39}Ar$ on plagioclase phenocrysts, "Laboratoire Magmas et Volcans", Université Blaise Pascal, France). This places the growth of Nevado Ampato and Nevado Sabancaya during late Pleistocene to Holocene.

Activity at Nevado Sabancaya during Holocene was dominated by lava flows and lava domes with few occurrences of pyroclastic deposits (de Silva and Francis 1990; Thouret et al. 1994). The Sabancaya block lava flows are thick and extend as far as 8 km from the summit towards the W to SE (Fig. 1c). A lava flow, emplaced on the western slope of the volcano and locally covering a peat bog (Fig. 1c), is 5,440±40 years B.P. old, as given by ^{14}C dating of the buried organic matter (Thouret et al. 2001). This suggests that the main effusive activity of Nevado Sabancaya is middle to upper Holocene in age (Fig. 1c). A few pyroclastic-flow deposits also point to some Holocene explosive activity. For example, a tephra layer, contained within a peat bog located near Sallalli (Fig. 1c), can be related to a 8,500 years old hydromagmatic eruption (Juvigné et al. 1998). The thickness of tephra layers related to explosive activity at Nevado Sabancaya is small, suggesting modest volumes of tephra (10^3–10^4 m^3) and consequently low magma production rates (10^6–10^7 m^3 per year).

The recent eruptive activity ended a dormant period of about 200 years. The last recorded volcanic activity occurred during the 18th century, as suggested by Spanish chronicles. Since then, Nevado Sabancaya was characterised by weak solfataric activity from vents within and outside the summit crater.

The 1990–1998 eruptive activity Fof Nevado Sabancaya

The most recent crisis started in December 1986 by increased fumarolic activity. Frequent pulses of steam, minor ash emission and a strong sulphur odour were reported in June 1988 (GVN 1988). Annular cracks were observed on the summit ice cap. The activity then gradually increased. At the end of May 1990, following a few days of intense seismic activity, the major crisis (VEI 2–3) began on May 29th (GVN 1990). Violent explosions generated 1–5-km- and exceptionally 7-km-high ash plumes. Ash fall was dispersed as far as 12 km from the summit. The portable seismic network, which had temporarily monitored the volcano, measured 10–15 events per day in September 1990 and as many as 50 in October 1990, which were centred about 10 km NE of the crater (Thouret et al. 1994). The activity consisted of alternating moderate-magnitude (VEI 2) vulcanian and hydromagmatic events.

During the first two years (1990–1992), explosions occurred every 20–30 min on average (Fig. 2a), lasted about 1 min and produced 3–4-km-high grey ash plumes (GVN 1990 to 1992). During 1993–1994, repose time between two eruptions increased from 30 min to about 2 hours, the ash plumes were light to medium grey and rarely white and they only reached average heights of 2–3 km (GVN 1994). Since 1995, the frequency of explosions gradually decreased to 5–6 events per day, with 1–3-km-high light grey to white plumes (GVN 1995, 1997). After 1997, the volcano exhibited a very discontinuous activity, with white or rarely grey plumes, which never exceeded 300–500 m in height (GVN 1998, 2000).

The mean production rate of magma is low, less than 10^7 m^3 per year. The bulk volume of the tephra emitted during the climactic phase of the eruption from May to October 1990 has been estimated at 0.025 km^3 (GVN 1994; Thouret et al. 1994). The 1990 tephra contained 85–90% lithic clasts (GVN 1991; Thouret et al. 1994). Since late 1990, juvenile fragments progressively increased to 40–50% in 1992 (Fig. 2a). The juvenile component consisted of glassy, slightly vesicular black to grey material (GVN 1994). The ballistic ejecta included dense, slightly vesicular blocks with radial cracks and scarce bread-crust bombs, which suggest the eruption of degassed juvenile magma and fragmentation due to phreatomagmatic processes.

Textures and petrology of juvenile material

The erupted juvenile material consists of dark, slightly vesicular and highly porphyritic andesites and dacites. Rare fine-grained mafic magmatic enclaves are contained within some of the juvenile tephra ejected since 1992. None have been found in the samples collected in 1990.

a

	1990-1992	1993-1994	1995-1997	Post 1997
Frequency of eruptions	every 20-30 minutes	Every 1-3 hours	5-6 events per day	< 5 events per day
Height of ash plumes	3 to 5 km high, rarely 7 km high	2-3 km high	1-3 km high	<1 km, 300-500 m high in average
Colour of plumes	light grey to grey	light-medium grey rarely white	light grey to white	mainly white
Dispersion of ash	about 10 km, rarely as much as 12 km		< 5 km	< 1 km
Percentage of juvenile fragments	10-15% in1990 to 40-50% in 1992	40-50 %	slight decrease	no juvenile tephra
Main eruptive activity	vulcanian and hydromagmatic		vulcanian, phreatomagmatic	phreatic or fumarolic

b

	1990		1992 - 1994	1995 - 1997
Vesicularity	moderately vesicular (10-15 vol.%)	*No sampling during 1991*	moderately vesicular (5-10 vol.%), few dense blocks	poorly vesicular (<5 vol.%), frequent dense blocks
Vesicle shapes	large amoeba-like		large amoeba-like to small subrounded	small subrounded
% phenocrysts	◄- - - - - - - -		20-25 vol.%	- - - - - - - - ►
Phenocryst textural characteristics	**DACITE** clear plagioclase no reaction rims		**ANDESITES** clear plagioclase + "dusty-rimmed" plagioclase (variable amount) reaction rims around amphiboles and biotites	
Magmatic enclaves	none identified		10 to 5 cm angular to subrounded	< 5 cm subrounded

Fig. 2a, b a Summary of the main characteristics of the 1990–1998 eruptions of Nevado Sabancaya. **b** Summary of the main textural and mineralogical characteristics of the erupted juvenile products expelled during the 1990–98 eruption

Textures

In hand specimen, juvenile material is generally porphyritic and moderately to poorly vesicular. The most vesicular material (10–15 vol%) was produced during the first eruptive episodes in 1990 (Fig. 2b). The 1992–94 tephra are mainly moderately vesicular (5–10 vol%) with only a small proportion of non-vesicular dense blocks. The juvenile blocks from later events are characterised by lower vesicularity (<5 vol%) with a predominance of dense blocks. The variation in vesicularity is correlated with vesicle-shape and size from large amoeba-like to small subrounded vesicles (Fig. 2b). These textural characteristics suggest either the eruption of a more degassed magma or an increasing occurrence of phreatomagmatic events.

The juvenile material is porphyritic with 20–25 vol% phenocrysts (>200 μm) and microphenocrysts (200–80 μm) within a highly crystalline groundmass (Fig. 3). The phenocryst assemblage mainly consists of plagioclase (about 80–85 vol% of the phenocrysts), associated with high-Ca pyroxene, hornblende, biotite, and iron-titanium oxides. Microphenocrysts of low-Ca pyroxene are also found within the most evolved dacitic lavas ejected during the 1990 events (64 wt% SiO_2, Table 1). The fine-grained groundmass (<80 μm) consists of plagioclase, high-Ca pyroxene, amphibole, iron-titanium oxides, and scarce colourless to brownish interstitial glass.

Plagioclase compositions

Textures and compositions of the plagioclase phenocrysts are variable and define two main populations: clear plagioclase phenocrysts and “dusty-rimmed” plagioclase phenocrysts (Figs. 3a, b). Variable amounts of both phenocryst populations are found in lavas (Fig. 2b). The 1990 dacite contains mostly clear plagioclase phenocrysts (less than two “dusty-rimmed” plagioclase phenocrysts per thin section). Andesites contain variable amounts of clear and “dusty-rimmed” plagioclase phenocrysts, with a marked predominance of the “dusty-rimmed” type. There is no systematic correlation between the relative quantity of the two types and the time of eruption.

The clear plagioclase phenocrysts are sodic, ranging from An_{25} to An_{45} with a higher frequency of $An_{25–35}$ compositions ($\geq$70% of the population, Fig. 4c). They are not optically zoned and they do not show any composi-

Table 1 Representative major element analyses

Sample No.	Average andesite	sab2	sab3	sab3b	GS921	sab9215	sab9216	GS931	sab941a	sab942	sab943	sab944	sab952a	sab953	sab959	sab969	sab9717	sab9718	sab9719	sab9218	sab941b
Date	Holocene	1990	1990	1990	1992	1992	1992	1993	1994	1994	1994	1994	1995	1995	1995	1996	1997	1997	1997	1992	1994
Type	Lava flows	Tephra	Tephra	Tephra	Tephra	Tephra	Tephra	Tephra	Tephra	Tephra	Tephra	Tephra	Tephra	Tephra	Tephra	Tephra	Tephra	Tephra	Tephra	Enclave	Enclave
SiO_2	61.64 (.55)	63.10	60.95	61.69	60.10	60.80	60.30	61.87	62.36	61.78	62.33	61.87	62.13	62.29	62.00	61.90	61.47	61.63	62.02	57.70	56.77
TiO_2	0.98 (.02)	0.87	1.06	0.93	1.08	1.03	1.45	0.97	1.04	0.97	1.00	1.02	0.99	0.97	0.99	0.94	0.98	1.00	0.98	1.35	1.35
Al_2O_3	15.77 (.27)	15.30	15.70	15.68	15.90	15.90	16.10	15.70	15.52	15.54	15.75	15.53	16.18	16.10	15.90	16.37	16.12	16.41	16.39	16.60	16.69
Fe_2O_3	5.83 (.31)	5.17	5.95	5.86	6.05	5.95	6.40	5.76	6.12	5.83	5.94	6.21	5.87	5.69	5.95	5.48	5.69	5.88	5.71	7.43	7.81
MgO	2.87 (.31)	2.34	2.82	2.77	2.93	2.76	2.70	2.52	2.70	2.52	2.62	2.63	2.55	2.53	2.50	2.47	2.51	2.57	2.53	3.38	3.60
CaO	5.22 (.36)	4.63	5.63	5.02	5.75	5.51	5.70	4.97	5.23	5.27	5.21	5.42	5.12	4.95	5.00	4.85	5.02	5.09	5.03	6.71	7.16
Na_2O	4.40 (.19)	4.30	4.34	4.17	4.60	4.60	4.95	4.56	4.05	4.45	4.14	4.39	4.53	4.31	4.17	3.78	3.82	3.98	3.89	4.67	4.23
K_2O	2.83 (.14)	3.13	2.57	2.82	2.75	2.70	2.85	2.98	2.84	2.91	2.82	2.84	2.93	2.78	2.85	2.89	2.87	2.78	2.88	2.35	2.11
MnO	0.07 (.01)	0.07	0.08	0.08	0.08	0.07	0.08	0.07	0.08	0.07	0.08	0.08	0.07	0.07	0.08	0.07	0.07	0.07	0.07	0.08	0.09
P_2O_5	0.38 (.01)	nd	0.41	0.33	nd	nd	nd	nd	nd	nd	nd	nd	nd	nd	0.33	0.28	0.33	0.32	0.31	nd	nd
LOI	0.12 (.10)	0.12	0.01	0.32	0.00	0.02	0.00	0.08	0.09	0.10	0.08	0.05	0.02	0.00	0.03	0.03	0.00	0.00	0.00	0.00	0.07
Sum	100.11	99.03	99.52	99.67	99.24	99.34	100.53	99.48	100.03	99.44	99.97	100.04	100.39	99.69	99.80	99.05	98.88	99.73	99.81	100.27	99.88

The first column gives an average of seven samples of Holocene block lava flows with standard deviations in brackets. The analyses of samples from the eruptive events until 1994 were supplied by the "Laboratoire Magmas et Volcans" of the Université Blaise Pascal, Clermont-Ferrand, France (ICP AES method), while later samples were analysed at the "Ecole des Mines de Saint-Etienne" (XRF method). Duplicate analyses were performed to prevent any bias between the two laboratories. All major elements variations are within error

tional gradient from core to rim (Fig. 4b). Their compositional profiles reveal low-amplitude oscillatory zoning ($\leq$10 mol% An oscillations, Fig. 4b). High resolution backscattered electron images obtained with the microprobe on the clear plagioclase phenocrysts do not identify any resorption surfaces, suggesting continuous growth of plagioclase. The low amplitude oscillations in plagioclase may be due to local kinetic effects in a boundary layer at the crystal-melt interface, as previously demonstrated by experimental and theoretical studies (Lofgren 1980; Allègre et al. 1981; Anderson 1984; Pearce 1994; Ginibre et al. 2002). The oscillations could be explained by competition between high growth rates and much slower element diffusion in the melt, which allow a chemical boundary layer to repeatedly grow and be destroyed. Consequently, the clear plagioclase most probably crystallized within a dacitic melt under slightly variable physical and chemical conditions.

The "dusty-rimmed" plagioclase phenocrysts are characterised by inversely zoned dusty phenocrysts (Fig. 3, Fig. 4c). They exhibit an inclusion-free core and a concentric zone rich in tiny melt inclusions, which is delimited by a wavy dissolution surface. The resorption surface separates an oscillatory-zoned sodic core ($An_{25–45}$) and a Ca-rich oscillatory-zoned "dusty" mantle ($An_{45–65}$). An outermost inclusion-free rim$\leq$50 μm wide of $An_{45–60}$ generally occurs in textural and compositional continuity with the "dusty" zone (Fig. 4b, c). The compositional shift between clear cores and dusty mantles suggests that the phenocrysts first nucleated in a dacitic melt, then completed their growth in a more calcic magma (Fig. 4a, b). Entrapment of melt inclusions and the wavy limit separating cores from rims suggest that the crystals underwent a resorption episode, consistent with significant magma temperature increase and composition changes related to magma recharge events (Barbarin 1990; Davidson and Tepley 1997; Seaman 2000). Consequently, the dusty plagioclase population in the Nevado Sabancaya andesites is the possible indicator of andesite-dacite magma interaction within the reservoir.

Microphenocrysts of plagioclase (80–200 μm) in andesites span an $An_{40–60}$ compositional range (Fig. 4), whereas they present a narrower range ($An_{40–50}$) in the 1990 dacite. They are very weakly normally zoned from core to rim. They are texturally clear crystals, and often exhibit sub-rounded shapes. Plagioclase microlites are abundant in the groundmass of lavas, which is highly microcrystalline. Their compositions range from An_{30} to An_{35} in the dacite, and from An_{30} to An_{55} in the andesites.

Compositions of mafic minerals

Amphibole occurs as large euhedral phenocrysts (>200 μm), as euhedral inclusions in clear plagioclase phenocrysts, as microphenocrysts (80–200 μm) and within reaction rims around biotite crystals. Destabilisation features of hornblende and biotite (resorption or dissolution surfaces, reaction rims) are frequent and nearly

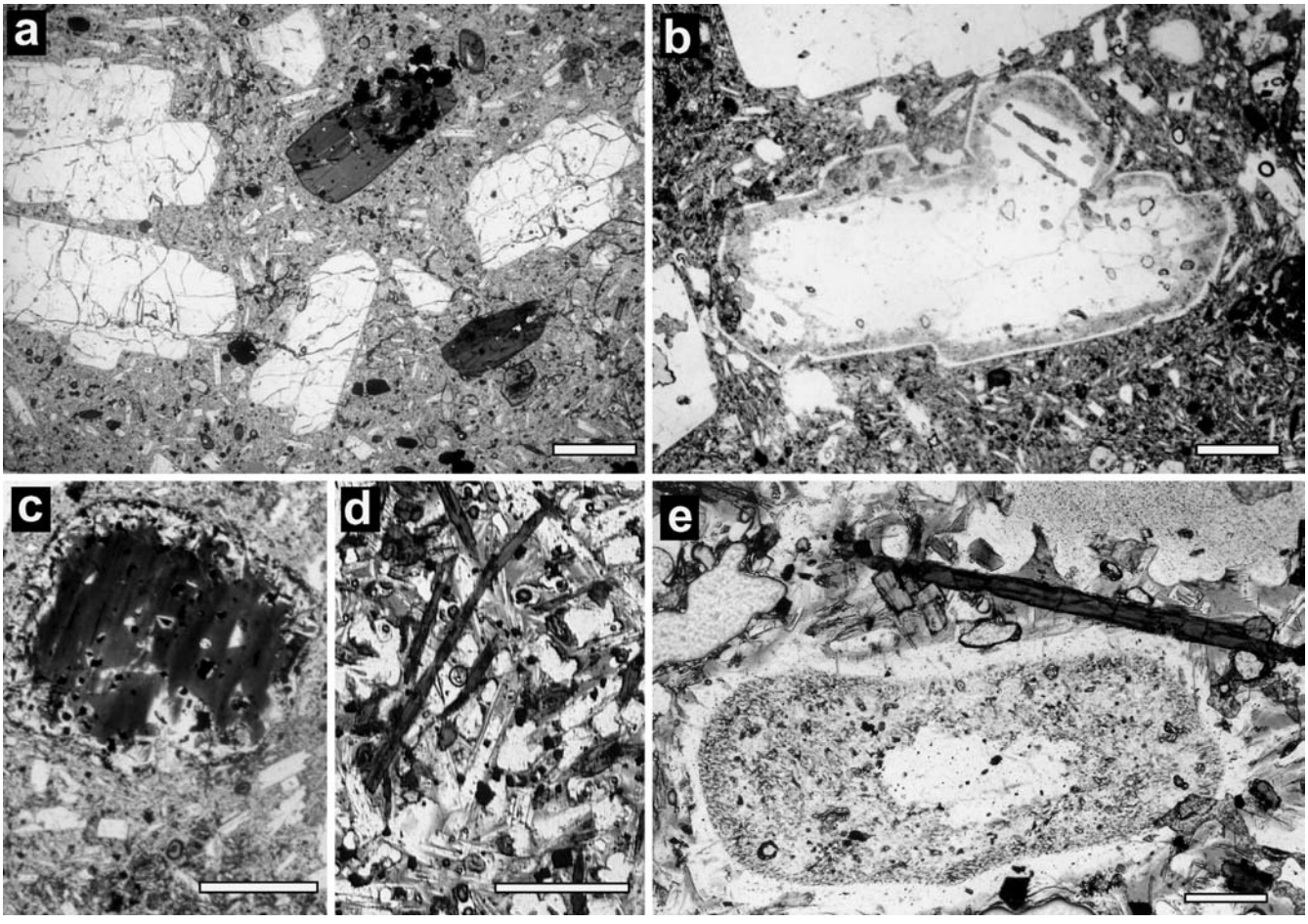

Fig. 3a–e Photomicrographs of thin sections of lavas and associated magmatic enclaves. The *white horizontal bar* represents 500 μm for images **a, b, c** and **d** and 100 μm for **e**. **a** Textures of the early-emitted dacite showing clear plagioclase phenocrysts and stable amphibole with sharp edges and euhedral shapes, **b** "dusty-rimmed" plagioclase phenocryst in andesite, **c** rounded and embayed biotite phenocryst in andesite surrounded by reaction rim, **d** fine-grained enclave showing a quench-textured groundmass consisting of acicular and hollow crystals of plagioclase and amphibole, **e** dusty plagioclase phenocryst within a magmatic enclave

ubiquitous in the juvenile material, except within the early-erupted dacite, where they show sharp edges and euhedral shapes (Fig. 3a). In andesites, amphibole phenocrysts are rounded and embayed, suggesting a resorption process, and are surrounded by reaction rims of variable size (10–50 μm wide), mainly consisting of tiny crystals (5–10 μm) of iron-titanium oxides, sometimes associated with plagioclase and orthopyroxene. Biotite phenocrysts also exhibit reaction rims (Fig. 3c), which are commonly wider (up to 150 μm) and contain hornblende in addition to other minerals. In juvenile material, amphibole defines two distinct compositional populations (Fig. 5). The euhedral phenocrysts and the euhedral inclusions in clear plagioclase phenocrysts exhibit a homogeneous magnesio-hornblende composition (IMA classification, Leake et al. 1997) and do not show any discernible zoning from core to rim. Al_2O_3 and TiO_2 contents range between 6 to 10 and 1–2.5 wt% respectively, with Al^T/Si ratios ranging between 0.15–0.25 (Fig. 5). Conversely, amphibole in biotite reaction rims plot within the magnesio-hastingsite compositional field, with Al_2O_3 and TiO_2 contents and Al^T/Si ratios ranging between 11 to 14, 3–4.5 and 0.3–0.4 wt%, respectively. These compositions are similar to those of crystals found in the enclaves (Fig. 5).

Ca-rich pyroxene phenocrysts compositions are similar and span a diopside — augite range ($Wo_{46}En_{39}Fs_{15}$–$Wo_{40}En_{45}Fs_{15}$; Morimoto et al. 1988). They exhibit no discernible compositional zoning. Clinopyroxene microlites in the groundmass span a larger compositional range in the augite field, show a calcium depletion trend and are associated with rare Ca-poor pyroxene microlites ($Wo_3En_{75}Fs_{22}$–$Wo_2En_{68}Fs_{30}$).

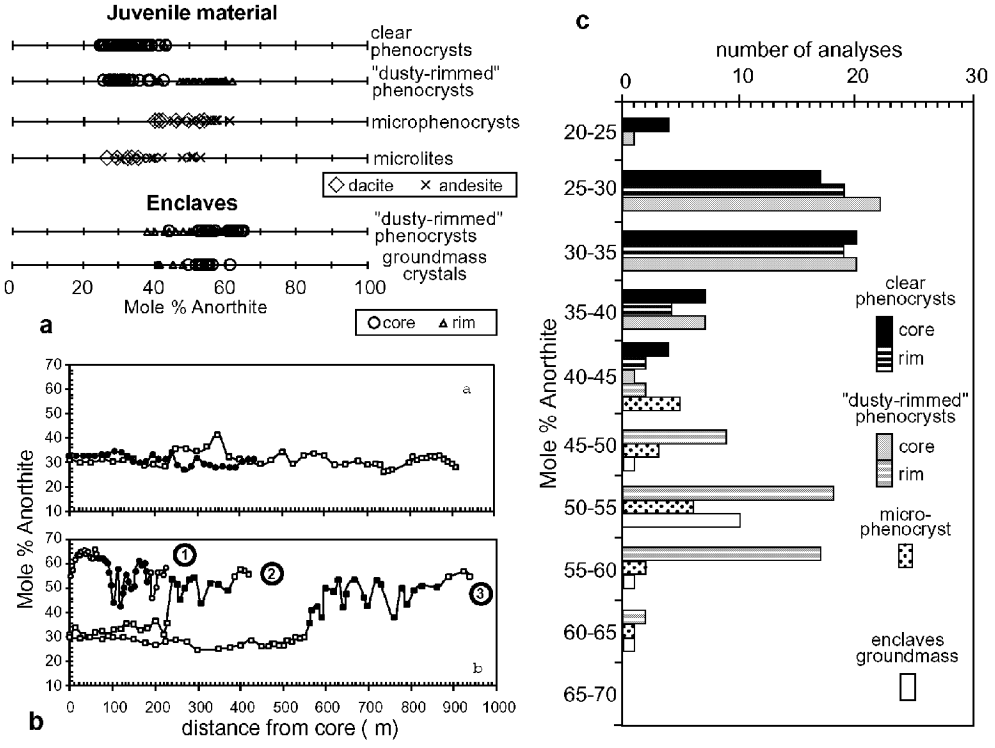

Fig. 4a–c Plagioclase compositions as mole% anorthite to illustrate differences among the various plagioclase populations of juvenile tephra and associated magmatic enclaves. **a** Core and rim compositions of clear and "dusty-rimmed" plagioclase phenocrysts, microphenocrysts and microlites in dacite and andesites, and "dusty-rimmed" phenocrysts and groundmass crystals in enclaves. **b** Compositional profiles were realized in plagioclase phenocrysts with a spacial resolution of 10–20 μm and an analytical precision of approximately ±1 mol% An. **a** clear phenocrysts in juvenile tephra; **b** dusty phenocrysts in enclaves (1) and in juvenile tephra (2 and 3). Inclusion-rich zone within "dusty-rimmed" plagioclase is shown by *black dots*. Clear phenocrysts exhibit a low-amplitude oscillatory zoning due to kinetic effects in a boundary layer at the melt-crystal interface. The "dusty-rimmed" phenocrysts in juvenile tephra show dissolution surfaces, accompanied by a major compositional step, which is compatible with a temperature increase and composition changes related to magma recharge events. Cores of dusty phenocrysts in enclaves are possible relics of phenocrysts from the mafic magma brought up by recharge events. **c** Histograms of plagioclase compositions, showing that the cores of dusty phenocrysts in juvenile tephra span the same compositional range as the clear phenocrysts, whereas their rim compositions are very similar to those of the groundmass crystals of the enclaves

Textures and petrology of magmatic enclaves

Textures of enclaves

Rare fine-grained andesitic enclaves are found within juvenile tephra expelled from 1992 to 1997 (Fig. 2b). Their abundance is difficult to estimate due to their scattered occurrence in the pyroclasts. However, from our sampling they seem rather scarce (<<0.1% vol, as documented in Bacon 1986). They range in size from a few mm to 10 cm in diameter. In samples from late eruptive episodes, they are $\leq$3 cm. They are typically angular, although subrounded enclaves also occur. They have sharp and smooth edges, do not exhibit crenulated contacts with host, and also lack chilled margins.

The fine-grained enclaves are poorly and finely vesicular and are phenocryst-poor (<1 vol%). Randomly oriented interlocking columnar or acicular crystals, with interstitial colourless to brownish glass and few voids, define a quench-textured groundmass (Fig. 3d). The groundmass crystals mainly consist of plagioclase, with lesser amount of amphibole and iron-titanium oxides. Groundmass plagioclase crystals are clear. Small rounded vesicles are ubiquitous within the interstitial glass, in variable proportions from one sample to another. There is no correlation between enclave size and groundmass crystal size, and there is no decrease in grain-size towards the contact (no chilled margins).

Mineral compositions

Groundmass plagioclase have calcic cores ($An_{50–60}$), and are slightly normally zoned towards the rims ($An_{40–50}$, Fig. 4a). Scarce plagioclase phenocrysts invariably show an inclusion-rich concentric zone (Fig. 3e). In most case, they are compositionally different from the "dusty-rimmed" plagioclase in their host (Fig. 4a). Their calcic cores are compositionally homogenous ($An_{50–65}$). Their "dusty" mantle and outermost inclusion-free rim span a wider compositional range ($An_{40–60}$) and they are oscillatory-zoned (Fig. 4b). Compositional profiles show

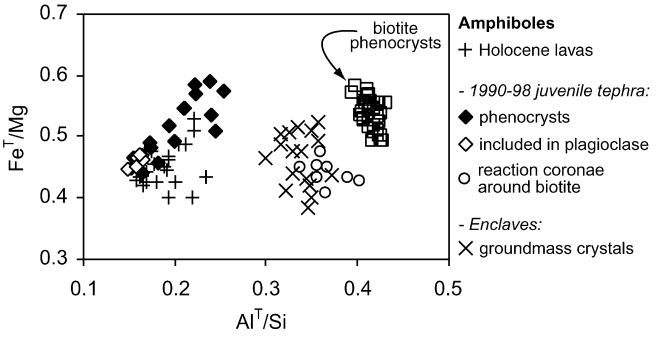

Fig. 5 Fe/Mg plotted against Al/Si to illustrate differences in composition among amphiboles in the magmatic enclaves and the juvenile tephra. Amphibole in the Holocene andesites spans a similar compositional range as the 1990–1998 juvenile tephra. Amphibole crystals within the reaction coronae around biotite are similar to those in magmatic enclaves

higher-amplitude oscillations (15–20 mol% An) within their "dusty" mantle compared to that from "dusty-rimmed" plagioclase in host rocks (Fig. 4b). Only two "dusty-rimmed" crystals with sodic core similar to that of host rocks were found in the enclaves, and they are considered as host-derived xenocrysts.

Groundmass amphibole occurs as acicular crystals, with aspect ratios as high as 20. It plots within the magnesio-hastingsite compositional field (Leake et al. 1997). They have higher Al_2O_3 and TiO_2 contents and Al^T/Si ratios (11–13, 2.5–4.5 and 0.3–0.4 wt%, respectively) than hornblende phenocrysts in host rocks (Fig. 5) and they are similar to amphibole in reaction rims around biotite in host rocks. Scarce xenocrysts of lower-Al amphibole, similar in composition to amphibole phenocrysts in the host rocks, and scarce pyroxene xenocrysts show accentuated embayed shapes surrounded by reaction rims.

Experimental works have demonstrated that crystal shapes are related to the cooling history of magmas (Lofgren 1980): the higher the cooling rates, the more elongate the crystals are prone to be. They have shown that high aspect ratio crystals (columnar to acicular shapes) are characteristic of quenched textures and represent textural evidence of magma crystallization in an undercooled state (Lofgren 1974; Lofgren 1980; Koyaguchi 1986; Bacon 1986). Consequently, the textural features of enclaves are compatible with a magmatic origin, and the composition of their groundmass plagioclase and amphibole suggest that they crystallise from an andesitic magma. The quenched textures and the presence of host-derived xenocrysts in the enclaves provide empirical evidences for interaction between coexisting magmas (Bacon 1986, Tepley et al. 1999). Nevertheless, a mingling of andesitic magma blobs dispersed within dacitic magma would hardly explain the lack of decrease in grain-size towards the contact with host, the lack of crenulated contact and the angular shape of enclaves. Consequently other processes may be involved in their formation and their genetic relationships with host magmas will be examined in the discussion section.

Pre-eruptive geobarometry and geothermometry conditions

Estimation of pre-eruptive magma storage conditions (P, T, X_{H2O}) is required to constrain and interpret the processes producing the 1990–1998 eruption. An accurate and direct way to evaluate storage pressure is to determine magma chamber depth using geophysical methods. Unfortunately, during the eruptive crisis, the seismic monitoring was not suited to define any spatial localisation of the magma storage zones beneath the volcano. Another way is the use of geobarometers based upon compositional variations of mineral phases sensitive to pressure changes. The "Al-in hornblende" barometer, which provides an empirical and experimentally investigated linear correlation between pressure and total aluminium content in hornblende grown within calc-alkaline magmas, gives a mean pressure range of 200–350 MPa for the phenocryst cores of lavas. This pressure range reflects both the variation of Al_2O_3 content of amphiboles in lavas (Fig. 5) and the calibration differences of the barometer (Hammarstrom and Zen 1986; Hollister et al. 1987; Johnson and Rutherford 1989; Schmidt 1992). Although these pressure estimates appear realistic and reasonable, an error of at least 100 MPa must be considered.

Pre-eruptive temperatures were estimated using the Fe-Ti oxide geothermometer. They were calculated with the scheme of Spencer and Lindsley (1981) for pairs of magnetite and ilmenite that satisfied the equilibrium Mg-Mn partitioning test (Bacon and Hirshmann 1988). Only homogeneous oxide crystals in contact with the groundmass glass were considered, and several pairs were analysed in each sample. The pre-eruptive temperature estimates for the magmas expelled during the 1990–1998 crisis are 940±50 °C, with an average temperature of 940±30 °C for the dacitic melts of the 1990 early stage, 990±40 °C for the 1992 lavas, and 920±30 °C for the post-1993 lavas.

Geochemistry of the products

Whole-rock major and trace element geochemistry

The compositions of juvenile tephra and magmatic enclaves are shown in Figs. 6, 7 and 8, and representative analyses are given in Tables 1 and 2. Consistent with the observed modal mineralogy, the juvenile rocks do not span a wide range of compositions. They vary between 60 and 64 wt% SiO_2 while the magmatic enclaves exhibit homogeneous compositions around 57 wt% SiO_2 (Table 1). The suite is andesite-dacite with high-K calc-alkaline affinity (2–3 wt% K_2O), which is a constant feature of the Quaternary magmatism in the Central Andes, and southern Peru (Gill 1981). While SiO_2 contents do vary slightly, the juvenile tephra do not show any systematic variation with time (Fig. 6a). The most differentiated rock is the enclave-free and "dusty-rim-

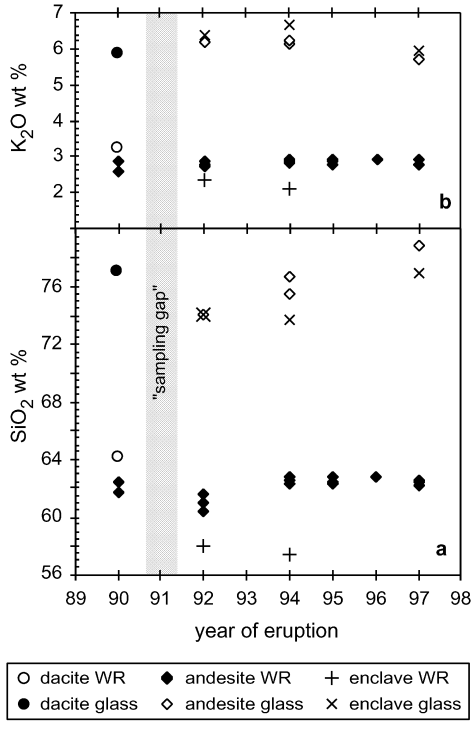

Fig. 6a, b Evolution of SiO_2 content (**a**) and K_2O content (**b**) of whole rocks and groundmass glasses during the 1990–1998 eruptions

med" plagioclase-free dacite erupted in 1990. It was erupted together with enclave-free andesites spanning a 61.5–62.5 wt% SiO_2 range. Andesites from the 1992 eruptive events are the least differentiated with a SiO_2 range of 60.5–61.5 wt%. Andesites erupted after 1993 show a constant composition around 62.5 wt% SiO_2. Recent andesitic lavas from the Holocene effusive activity show a very narrow range of composition around 62 wt% SiO_2, comparable to the post-1992 compositions (Table 1). Fine-grained magmatic enclaves are generally 1 or 2 centimetres in size and thus difficult to extract from their host for whole-rock chemistry. Two larger enclaves were separated and analysed (Fig. 6a). Their chemical compositions are similar (57.5–58 wt% SiO_2), although their hosts are chemically different. The enclave with the highest silica content is found within the least differentiated andesite, erupted during the 1992 eruptive events.

Harker-type diagrams exhibit linearity for most oxides and trace elements, although some of the plots show a slight scatter (Figs. 7, 8). MgO, CaO, FeOt, TiO_2, and Sr exhibit negative correlations with SiO_2, whereas K_2O and Rb show positive trends (Figs. 7, 8). Al_2O_3 also decreases with increasing SiO_2, but some of the analyses plot off the general trend. Na_2O does not display any systematic evolution with increasing SiO_2 content, and show a significant scatter of values, which cannot only be attributed to analytical imprecision. V and Sr concentra-

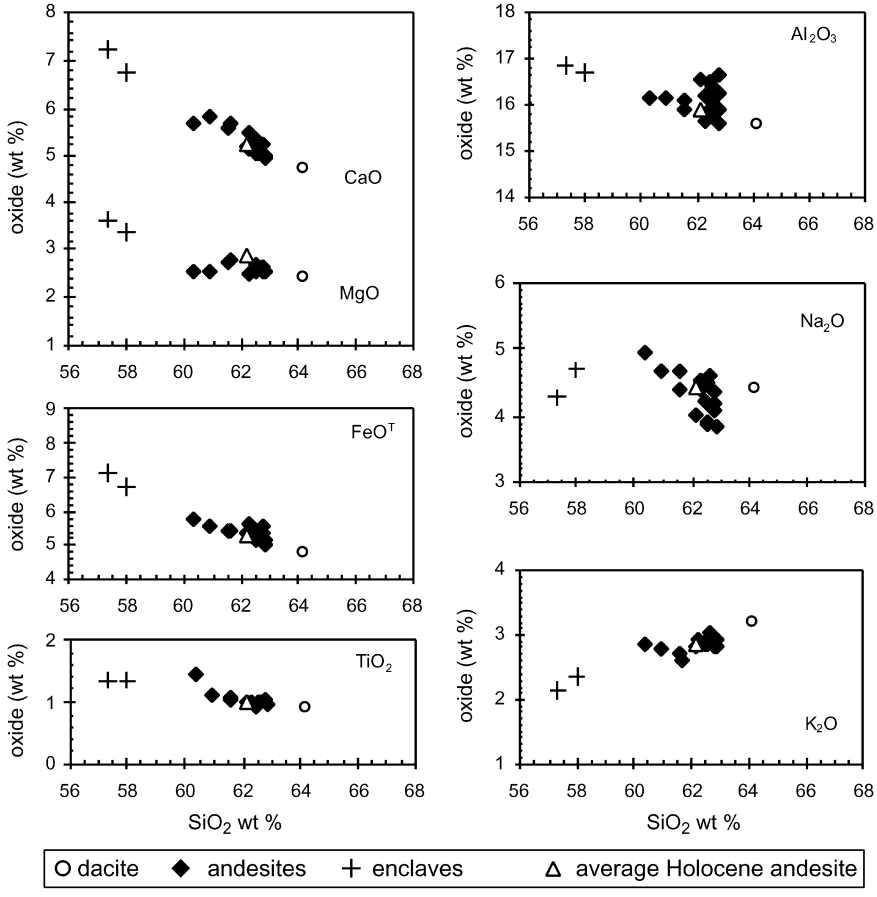

Fig. 7 Harker-type diagrams for major elements in juvenile tephra and associated magmatic enclaves of the 1990–1998 eruptions. An average composition of Holocene block-lava flows is also shown

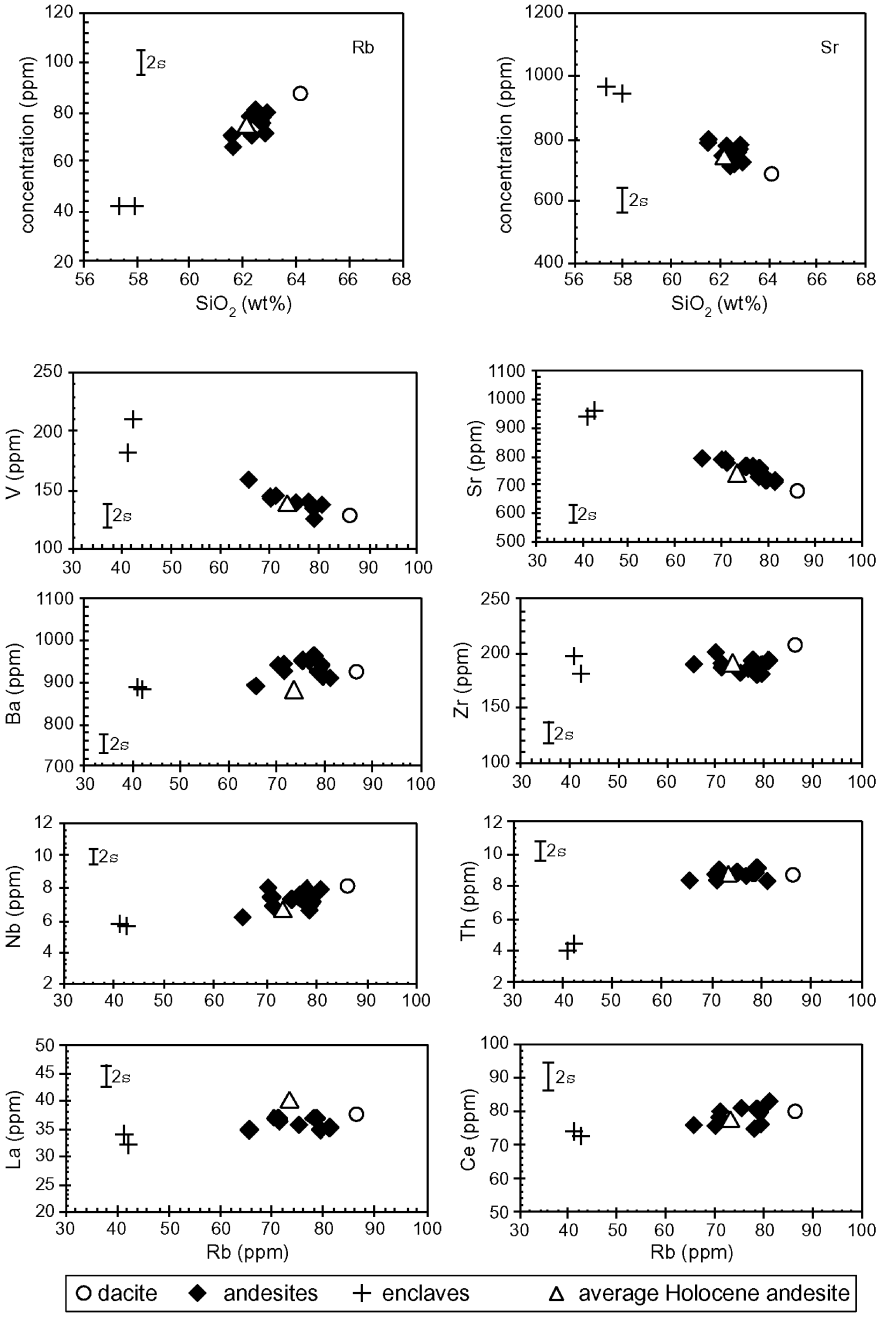

Fig. 8 Harker-type diagrams for trace elements in juvenile tephra and associated magmatic enclaves of the 1990–1998 eruptions. An average composition of Holocene block-lava flows is also shown

tions show a clear negative correlation with Rb, while the other trace elements are positively correlated (Fig. 8). A closer inspection reveals more complex evolution trends. While the compositional trends are linear for andesites and dacite on most diagrams, the magmatic enclave compositions plot off these linear trends (e.g. CaO, MgO, FeO versus SiO_2 and V, Sr versus Rb, Figs. 7, 8). On these diagrams, the whole series from enclaves to dacite plots on slightly incurved decreasing trends.

The involvement of crystal accumulation, fractional crystallization, and binary magma mixing may be debated from our chemical results. The juvenile material is porphyritic, but contains less than 30 vol% phenocrysts, mainly plagioclase. Plagioclase accumulation would result in correlation of CaO, Na_2O and Sr with the phenocryst contents, which is not observed in our study. Consequently a major role of crystal accumulation can be ruled out. The chemical evolution of the juvenile material and the enclaves, characterised by incurved negative trends for compatible elements and linear positive trends for the incompatible elements, suggests the influence of fractional crystallization to produce the dacitic magma. Nevertheless, the presence of inversely zoned "dusty-rimmed" plagioclase in andesites and the linear evolution from andesites to dacite may also account for magma mixing. In that respect, the juvenile andesites may re-

Table 2 Selected trace element analyses

Sample No.	Average andesite	sab2	sab3	sab9215	sab941a	sab942	sab943	sab944	sab953	sab969	sab9717a	sab9718	sab9719	sab9218	sab941b
Date	Holocene	1990	1990	1992	1994	1994	1994	1994	1995	1996	1997	1997	1997	1992	1994
Type	Lava flows	Tephra	Tephra	Tephra	Tephra	Tephra	Tephra	Tephra	Tephra	Tephra	Tephra	Tephra	Tephra	Enclave	Enclave
Rb	73.4 (4.5)	86.7	65.6	70.4	75.2	77.6	76.8	71.2	71.4	79.3	79.5	78.7	81.1	41.2	42.2
Sr	744.1 (62.8)	678.3	798.7	786.7	763.3	745.6	760.4	778.5	777.4	721.5	715	740.9	713.6	943.3	961.8
Ba	885.4 (51.4)	919.6	891.1	940.5	953	963.1	951.1	941.6	929.7	941.9	917.5	925.7	912.7	886.8	882.5
Sc	9.6 (0.6)	8.74	9.37	9.13	8.95	nd	nd	9.22	8.835	8.2	nd	8.14	7.99	10.36	12.21
V	139.0 (9.0)	127	158	143	138	nd	nd	143	145	124	nd	136	137	181	210
Cr	57.0 (15.0)	41	44	38.5	40	nd	nd	41	38	32	nd	37	37	46	59
Ni	20.6 (5.0)	21	26	25	26	18	17	25	23	21	15.5	23	22	36	34
Y	13.8 (0.7)	14.9	13.8	13.4	13.3	13.3	13.5	13.5	14.2	14	14.4	14.5	14	14.6	13.4
Zr	192.1 (8.7)	205.2	189.6	200.5	183.2	193.6	186	188.8	188.1	181.2	190.3	180.7	192.7	198.6	181.3
Nb	6.7 (1.2)	8	6.2	8	7.3	7.2	7.6	7.4	6.9	7.1	7.4	6.6	7.8	5.8	5.6
Ga	21.0 (0.7)	19.8	20.1	20.6	21.2	21.6	21.8	21.9	20.8	21.3	20.7	21.1	20.6	21.4	22.5
Th	8.7 (0.8)	8.6	8.4	7.9	9.4	nd	8.7	8.4	7.9	7.2	nd	8.9	8.3	4	2.5
Hf	6.7 (2.5)	9.2	7.1	5.2	5	4.4	6.7	3	5.8	1.1	4.5	4.1	5.7	8.6	6.1
La	42.2 (4.3)	37.3	34.7	36.9	33.6	34.3	nd	36.9	36.4	32.1	nd	31.1	30.6	33.9	28
Ce	78.9 (5.9)	79	76	75.5	72.3	75.2	nd	79.5	78.6	73.2	nd	70.8	70.1	73.9	65.6
Nd	39.1 (0.6)	36	38.1	38.4	30.3	31.4	nd	31.3	37.3	29.24	nd	29.1	26.8	40.5	34.2
Eu	1.5 (0.1)	1.42	1.58	1.51	1.32	1.29	nd	1.3	1.49	1.18	nd	1.3	1.19	1.73	1.58
Sm	8.3 (0.5)	7.67	8.25	7.61	5.65	5.87	nd	6.13	7.72	5.36	nd	5.39	5.03	8.27	6.24
Gd	4.8 (0.4)	4.19	4.63	4.53	3.66	3.69	nd	3.96	4.34	3.8	nd	3.72	3.59	5	4.73
Dy	2.6 (0.1)	2.8	2.85	2.77	2.25	2.28	nd	2.14	3	2.3	nd	2.26	2.22	2.83	2.41
Er	1.3 (0.2)	1.29	1.23	1.22	1.05	0.83	nd	1.03	1.2	1.2	nd	0.84	0.85	1.19	1.08
Yb	0.9 (0.0)	0.982	0.924	0.877	0.853	0.824	nd	0.925	0.962	0.88	nd	0.805	0.830	0.881	0.859

Samples were analysed at the "Ecole des Mines de Saint-Etienne". Sc, V, Cr, Ni, Y, Th and REE were obtained using a sequential ICP AES method and other trace elements were obtained using X-ray fluorescence on compacted powders

Table 3 Representative analyses of groundmass glasses

Sample	sab2	92–18	94–1a	94–3	97–19	92–18	94–1b	97–19
Type	Dacite	Andesite	Andesite	Andesite	Andesite	Enclave	Enclave	Enclave
Number of analyses	[8]	[5]	[3]	[7]	[3]	[1]	[4]	[6]
SiO_2	76.4 (1.3)	72.8 (0.8)	75.7 (0.6)	74.2 (1.8)	78.2 (0.4)	72.4	72.8 (0.5)	75.7 (0.8)
TiO_2	0.5 (0.1)	0.6 (0.1)	0.4 (0.3)	0.5 (0.1)	0.4 (0.05)	0.6	0.5 (0.3)	0.7 (0.2)
Al_2O_3	11.8 (0.8)	12.7 (0.5)	12.1 (0.5)	12.7 (0.9)	10.8 (0.2)	13.9	13.9 (0.3)	12.0 (0.5)
FeOt	1.1 (0.2)	1.5 (0.1)	1.3 (0.2)	1.2 (0.1)	1.1 (0.1)	1.6	1.5 (0.1)	1.3 (0.1)
MgO	0.2 (0.1)	0.1 (0.05)	0.06 (0.02)	0.1 (0.1)	0.04 (0.01)	0.1	0.1 (0.04)	0.1 (0.02)
MnO	0.03 (0.03)	0.03 (0.05)	0.00	0.1 (0.2)	0.05 (0.01)	0.00	0.01 (0.01)	0.01 (0.01)
CaO	0.5 (0.2)	0.5 (0.1)	0.2 (0.1)	0.4 (0.1)	0.5 (0.1)	0.3	0.4 (0.1)	0.3 (0.05)
Na_2O	2.9 (0.5)	3.2 (0.3)	2.9 (0.1)	2.8 (0.7)	2.6 (0.4)	2.7	3.1 (0.5)	2.4 (0.2)
K_2O	5.8 (0.3)	6.1 (0.1)	6.0 (0.2)	6.2 (0.6)	5.7(0.2)	6.3	6.6 (0.2)	5.9 (0.2)
Total	99.2	97.7	98.7	98.3	99.2	97.8	98.7	98.4

Major element analyses of glasses were obtained from thin sections using a Cameca SX100 electron microprobe in the "Laboratoire Magmas et Volcans" at the Université Blaise Pascal, Clermont-Ferrand (France). Operating conditions were 15 kV accelerating voltage, 8 nA beam current, 10 s counting times and a slightly defocused beam. The table presents the average compositions, with standard deviation in brackets, for groundmass and interstitial glasses of juvenile material and magmatic enclaves, respectively. The number of analyses used to calculate the average and the year of eruption are also reported. A defocused beam and low current are the best operating conditions to prevent loss of Na_2O and K_2O during the analysis. Volatile contents of the glasses are estimated by the deficit of the oxides sum and range from 0.8 to 2.2 wt%

present hybridised magmas. Coexistence of homogeneous hybrid andesites and magmatic enclaves may reflect complex mingling-mixing processes within the magma reservoir prior to eruption.

Groundmass glass compositions

Analyses of groundmass glasses were carried out by electron microprobe to examine the evolution of residual melts prior to solidification in both juvenile tephra and magmatic enclaves (Fig. 6). The volatile contents of these glasses, estimated by the deficit of the oxides sum (Table 3), are 0.8–2.2 wt%. The glasses are highly enriched in SiO_2 and K_2O, and depleted in other major elements compared to whole rocks. In a diagram of SiO_2 versus time of eruption (Fig. 6a), the residual groundmass glasses in lavas exhibit a temporal evolution, which generally parallels that of whole-rock silica contents. The 1992 juvenile tephra, which are the least differentiated lavas of the eruption, are also characterised by the least evolved groundmass glass. The later erupted tephra display an evolving trend towards more and more silica-rich glass compositions, whereas their bulk compositions are very constant.

Compositions of interstitial glasses in magmatic enclaves are similar to the groundmass glass compositions of their host. This homogeneity of interstitial glasses may be due to some melt exchange between enclaves and their host. Considering the contrasting compositions of mineral phases in enclaves and juvenile material, these exchanges may occur at a late stage. Furthermore, considering the occurrence of rare xenocrysts of plagioclase, pyroxene and amphibole and the composition of interstitial glass, the andesitic enclaves may represent a complexly evolved mixture rather than a pure magmatic end-member.

Isotopic data

Sr, Nd and O isotope ratios were determined for six samples of lavas and two enclaves (Table 4, Fig. 9). $^{87}Sr/^{86}Sr$ ratios of the lavas range from 0.7067 to 0.7069. They show an overall positive correlation with SiO_2 and are negatively correlated with their Sr content. The Sr isotope ratio of the 1990 dacite is the most radiogenic and the most depleted in Sr (Fig. 9). The magmatic enclaves exhibit similar Sr isotopic compositions (0.7067), which are the lowest $^{87}Sr/^{86}Sr$ ratios, which are correlated with the highest Sr contents. The Nd-isotope ratios cover a narrow range (0.51230–0.51237), but they also show a generally positive correlation with SiO_2. The dacite has the highest $^{143}Nd/^{144}Nd$ ratio and the enclaves the lowest (Table 4). $\delta^{18}O$ in lavas range from 7.6 to 8.4‰ VSMOW and are also positively correlated with SiO_2. The amplitude of $\delta^{18}O$ variation (0.8‰ for an SiO_2 increase of 2.5–3 wt%) is larger than ^{18}O-enrichment expected for closed-system fractional crystallization. AFC processes as well as crustal contamination may be responsible for such ^{18}O-enrichment. The positive trends between Sr- and O-isotope ratios and SiO_2 may be considered as mixing lines between a more radiogenic and ^{18}O-rich dacitic magma and recharge magmas with less radiogenic Sr and lower $\delta^{18}O$ compositions. Isotopic differences between the differentiated dacite and the magmatic enclaves are likely a result of repeated recharge events and subsequent AFC or crustal assimilation. Each input of more mafic magmas adds Sr with lower $^{87}Sr/^{86}Sr$ and O with lower $^{18}O/^{16}O$ ratios. Subsequent magma mingling/mixing processes then generate hybrid magmas with intermediate isotopic compositions and would tend to homogenize these compositions, although assimilation of more radiogenic and ^{18}O-rich crustal material may gradually increase their isotopic ratios. Repeated recharges, incomplete ho-

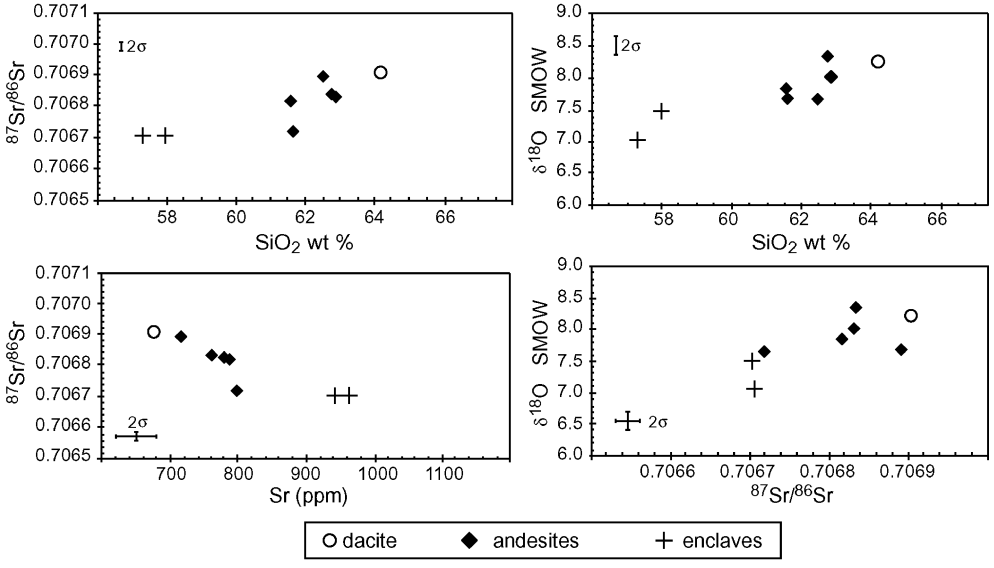

Fig. 9 Variation diagrams for Sr and O isotopic compositions of juvenile tephra and magmatic enclaves

Table 4 Isotopic compositions for selected samples

Sample N°	sab2	sab3	sab9215	sab941a	sab953	sab9719	sab-9218	sab-941b
Date	1990	1990	1992	1994	1995	1997	1992	1994
Type	Dacite	Andesite	Andesite	Andesite	Andesite	Andesite	Enclave	Enclave
$^{87}Sr/^{86}Sr$	0.706905	0.706719	0.706816	0.706835	0.706831	0.706894	0.706704	0.706705
1σ	0.000011	0.000013	0.000015	0.000014	0.000013	0.000012	0.000011	0.000013
εSr	34.14	31.50	32.87	33.14	33.09	34.00	31.29	31.30
$^{143}Nd/^{144}Nd$	0.512367	0.512362	0.512361	0.512338	0.512354	0.512357	0.512345	0.512301
1σ	0.000006	0.000005	0.000005	0.000008	0.000007	0.000009	0.00001	0.000011
εNd	-5.286	-5.384	-5.403	-5.85	-5.54	-5.48	-5.72	-6.57
$\delta^{18}O$	8.21	7.65	7.83	8.35	8.00	7.66	7.49	7.03

Sr and Nd isotopic analyses of whole-rock samples were performed at the "Laboratoire Magmas et Volcans" of Université Blaise Pascal, Clermont-Ferrand (France). After sample dissolution using an $HF/HNO_3/HClO_4$ mixture, Sr and Nd were separated using the procedures described in Pin et al. (1994) and Pin and Santos Zalduegui (1997). $^{87}Sr/^{86}Sr$ and $^{143}Nd/^{144}Nd$ isotopic ratios were determined using a VG Isomass 54E multicollector mass spectrometer. During the period of measurements, SRM-987 and La Jolla standards gave, respectively, $^{87}Sr/^{86}Sr = 0.71023 \pm 0.00002$ (2σ, n=6) and $^{143}Nd/^{144}Nd = 0.511852 \pm 0.000010$ (2σ, n=6). Oxygen isotope ratios of whole-rock samples were determined after degassing under vacuum on a silicate line for 3 hours at 250°C at Université Jean Monnet, Saint Etienne (France). The powders were reacted with BrF_5 at 550°C for 8 hours and the extracted O_2 converted to CO_2 using a hot platinised carbon rod (Clayton and Mayeda 1963). Duplicate splits of the internal quartz standard (Murchinson Line Quartz, MQ) were run with each batch of 6 samples. The $\delta^{18}O$ value of MQ has been determined to be 10.1‰ VSMOW (Vennemann and Smith 1990) after calibration against the NBS-28 quartz international standard, assuming a value for NBS-28 of 9.64‰ VSMOW (Coplen 1993). Oxygen isotope ratios were determined with a VG-prism mass spectrometer housed at the Ecole Normale Supérieure of Lyon (S.M.F. Sheppard). All data are reported in the familiar δ notation where $\delta^{18}O = (R_{sample} / R_{standard} - 1) \times 10^3$ and $R = {}^{18}O/{}^{16}O$. The average value obtained for MQ was used to normalise the $\delta^{18}O$ values on the SMOW scale. The average difference between 8 duplicates of MQ analysed during the course of this work was 0.3‰. This corresponds to a 1σ value of 0.2‰, which represents the approximate precision of the analyses

mogenisation and different degrees of crustal assimilation may explain the extended range of isotopic signatures. A recent study based on micro-drilling Sr-isotope analyses in complexly zoned plagioclase from calc-alkaline hybrid lavas demonstrated that the phenocrysts show systematic core-to-rim variations in $^{87}Sr/^{86}Sr$ ratios (Davidson and Tepley 1997). These changes are roughly correlated to major intracrystal perturbations such as dissolution surfaces and sudden jumps in An contents, which are caused by periodic magma recharges. These within-crystal isotopic variations are consistent with the observed bulk-rock isotopic variations, if subsequent crustal assimilation is postulated. In any case, the enrichment in radiogenic Sr and ^{18}O of the differentiated magma (the 1990 dacite) compared to the mafic recharge magma (as approximated from the magmatic enclaves) requires an open-system evolution within the upper crustal magma chamber.

Thus, the $^{87}Sr/^{86}Sr$ and $\delta^{18}O$ compositional ranges of the Nevado Sabancaya ejecta are not typical of mantle-derived magmas (0.703–0.704, and 6‰ SMOW) and imply subsequent assimilation of more radiogenic crustal materials. Crustal contamination will produce anomalous isotopic ratios and high abundances of incompatible elements, which are common features of the modern lavas of the CVZ (James 1984; Harmon and Hoefs 1984; Davidson et al. 1990). All authors now agree on the

existence of upper crustal contamination by AFC processes, but the nature of the source material is still unresolved: an asthenospheric mantle (isotopically depleted) or an enriched older lithospheric mantle. Some basaltic lavas (51.6–52.7 wt% SiO_2) from minor centres in southern Peru ca. 30 km WSW of Nevado Sabancaya are characterised by enriched isotopic signatures (Delacour et al. 2002), with $^{87}Sr/^{86}Sr$ ratios of about 0.707 and $\delta^{18}O$ spanning a 7.1–7.5 range, which are very similar to the magmatic enclave compositions. These basalts have mineralogical and compatible trace element compositions typical of poorly evolved magmas, suggesting they have been erupted quite rapidly from their source region without long residence within upper crustal magma chambers. Consequently, their distinctive isotopic characters reflect early stages of magma production and evolution within the lower crust, prior to subsequent evolution by AFC processes within shallow reservoirs. Several authors (Harmon and Hoefs 1984; Hildreth and Moorbath 1988) view contamination processes as occurring within partial melting zones at the base of the thick continental crust, with extensive assimilation, magma mixing, storage and homogenisation ("MASH" model).

Discussion

Origin and significance of the mixed populations of plagioclase

The mixed population of crystals in andesites and their geochemical characteristics suggest that the 1990–1998 juvenile andesites are mainly hybrid, and that magma mixing is involved in the magmatic evolution. The core compositions of "dusty-rimmed" plagioclase phenocrysts are similar to those of the clear plagioclase phenocrysts in the dacite (Fig. 4a), suggesting that they first nucleated within a dacitic melt whose composition was similar to the 1990 dacite. The wavy dissolution surfaces and the entrapment of melt inclusions testify that the crystals underwent a resorption episode in response to physical and/or chemical changes in the magma reservoir or conduit. The associated major compositional jump (Fig. 4b) indicates that this dissolution event is related to more mafic magma recharge and subsequent magma mixing (Allègre et al. 1981; Barbarin 1990; Singer et al. 1995; Tepley et al. 1999; Seaman, 2000). Experimental studies performed to reproduce such dusty textures and complex zoning within plagioclase phenocrysts demonstrate that temperature and chemical compositions are the determinant parameters to form these disequilibrium textures (Tsuchiyama 1985; Nakamura and Shimakita 1996; Nakamura and Shimakita 1998). Dissolution of plagioclase crystals occurs at temperatures above the liquidus of the initial solid solution. "Dusty-rimmed" plagioclases have been experimentally produced by partial dissolution due to reaction between Na-rich plagioclase already precipitated in a dacitic magma and anorthite-rich melt (andesitic melt), resulting in the formation of a Ca-rich mantle (Tsuchiyama 1985). Experimental results indicate that, in a hybrid lava produced by acid-basic magma mixing, the sodic plagioclase should undergo partial dissolution and reaction with the melt, forming dusty and mantled crystals, whereas the calcic plagioclase should react very little. Consequently, two distinct populations of clear plagioclase and one population of "dusty-rimmed" plagioclase might be expected in the hybrids: Ca-rich clear plagioclase from the mafic magma, Na-rich clear plagioclase from the acid magma and "dusty-rimmed" plagioclase due to the dissolution and reaction induced by the magma mixing. Hybrid andesites of Nevado Sabancaya may be manifestations of such magma-mixing processes involving more-mafic magma inputs within a dacitic magma batch. They show inversely-zoned "dusty-rimmed" phenocrysts, Na-rich clear phenocrysts, and Ca-rich clear microphenocrysts. Unlike in andesites, "dusty-rimmed" phenocrysts are very scarce in the 1990 dacite whereas clear unzoned Na-rich phenocrysts are very abundant, suggesting that the dacitic magma suffered only very limited interaction with the andesitic magma.

Petrological modelling

The hybrid origin of the andesites is assumed from mineralogical and geochemical data. Homogeneous hybrid andesites may result from mixing in variable proportions of a dacitic component with more mafic magmas, which are periodically supplied within the reservoir. The early-erupted dacite may be the differentiated component produced mainly by fractional crystallization and subsequent crustal assimilation, as shown by mineralogical, geochemical and isotopic data. The magmatic enclaves may represent the mafic component of the mixing but the presence of xenocrysts in the enclaves suggests that they suffered some interactions with the host magmas. In the vicinity of Nevado Sabancaya, no basalt is found and the most mafic products are Pleistocene andesitic lava flows which are similar in composition to the enclaves (Table 5). We performed and compared the petrological modelling of andesite / dacite magma mixing with both the magmatic enclaves and the Pleistocene lavas as mafic component. The results of mixing calculations using least squares regression of the major elements and subsequently trace elements are shown in Table 5. All calculations lead to low residuals, but considering the high degree of co-variation of major elements, apparent successful fits do not guarantee a unique petrologic model. The difference between the calculated and the observed compositions is small and lower than the analytical precision. For hybrid andesites with high silica content (62–62.5 wt%), the calculation leads to a large contribution from the dacitic end-member (around 65%), which may be problematic with respect to the mechanical behavior of magmas. Sparks and Marshall (1986) have predicted that homogeneous hybrids are formed if the temperature difference between magmas is low, and when the proportion of the silicic end-member is $\leq$50%, otherwise

Table 5 Results of binary mixing calculations

	Silicic component = 1990 dacite (sab2, table 1)							
	Mafic component composition		Hybrid 1			Hybrid 2		
			"Low-Si" andesite sab9215			"High-Si" andesite sab944		
	-A-	-B-						
	Pleistocene lava flow	Enclave sab9218	Observed comp.	Calculated comp. with mafic A	Calculated comp. with mafic B	Observed comp	Calculated comp. with mafic A	Calculated comp. with mafic B
SiO_2	57.99	57.98	61.59	61.60	61.61	62.26	62.12	62.13
TiO_2	1.26	1.36	1.04	1.04	1.08	1.03	1.02	1.06
Al_2O_3	17.37	16.68	16.11	16.30	16.02	15.63	16.25	16.00
FeOt	6.83	6.72	5.42	5.60	5.55	5.62	5.50	5.45
MgO	3.29	3.40	2.80	2.76	2.80	2.65	2.72	2.75
CaO	6.39	6.74	5.58	5.40	5.54	5.45	5.33	5.45
Na_2O	4.46	4.69	4.66	4.41	4.50	4.42	4.42	4.50
K_2O	2.31	2.36	2.73	2.82	2.84	2.86	2.88	2.90
MnO	0.10	0.08	0.07	0.08	0.07	0.08	0.08	0.07
Proportion of the silicic component				58.7%	58.9%		64.1%	64.4%
Proportion of the mafic component				41.3	41.1%		35.9%	35.6%
Sum of squares of residuals				0.15	0.06		0.14	0.09
Rb	44.8	41.2	70.4	69.4	68.0	71.2	71.7	70.5
Sr	833	943.3	787	742	787	779	734	773
Ba	942	886.8	941	929	906	942	928	908
V	171	181	143	145	149	143	143	146
Y	17.3	14.6	13.4	15.9	14.8	13.5	15.8	14.8
Zr	201	198.6	200	203	202	189	204	203
La	34.5	33.9	36.9	36.1	35.9	36.9	36.3	36.1
Ce	71.0	73.9	75.5	75.7	76.9	79.5	76.1	77.2
Nd	37.5	40.5	38.4	36.6	37.8	31.3	36.5	37.6
Eu	1.7	1.7	1.5	1.5	1.5	1.3	1.5	1.5
Yb	1.3	0.9	0.9	1.1	0.9	0.9	1.1	0.9

Binary mixing calculations were performed using least squares regression for the major elements of the 1990 dacite and either a 1992 enclave or a Pleistocene lava flow. All Fe is recalculated as FeO and analyses are normalised volatile free. All calculations lead to low residuals. Subsequently trace element compositions of the hybrid products are calculated and compared to the observed compositions. The difference between the calculated and the observed compositions is beneath the analytical precision

enclaves are formed. Thermal equilibration and subsequent crystallization increase mafic magma viscosity, preventing total homogenization. Despite small temperature differences between Nevado Sabancaya dacite and andesites, the calculated proportions do not seem realistic. Consequently, a simple two-component mixing does not represent a viable model, and multiple-stage mingling-mixing processes appear more realistic. Disaggregation of magmatic enclaves is also an efficient mechanism to enhance magma hybridisation (Clynne 1999). This mechanism may have contributed to the formation of the hybrid magmas through repeated recharge events within the Nevado Sabancaya magma chamber.

In any case, the occurrence of compositionally distinct hybrid andesites in the course of the eruption suggests that homogenisation was not completed prior to eruption. This may indicate that convective stirring was not sufficiently efficient to prevent segregation of melts, or that some mafic magma was introduced just before the eruption. Furthermore small disruptions of the system may promote some stirring on a local scale, which lead to multi-stage mixing of various end-members.

Origin of amphibole and biotite reaction rims

Amphibole breakdown and reaction coronae are common features in various types of magmatic rocks, especially within calc-akaline volcanics (Rutherford and Devine 1988; Rutherford and Hill 1993; Clynne 1999). They are currently attributed to solid-state amphibole dehydration, in response to water loss from the coexisting melt. The decrease of dissolved water results from either isothermal decompression during magma ascent or influx of low-H_2O and warmer magma in the storage region. Recent experimental work favours the first interpretation. Experiments on Mount St. Helens dacite have shown that amphibole stability requires a minimum of 4.2 wt% water and a pressure range of 120–160 MPa over a temperature range of 850–900 °C, which implies storage depths >6.5 km (Rutherford and Hill 1993). Decompression experiments for this temperature range have demonstrated that amphibole without reaction rims are obtained only for very rapid ascent (equivalent to 8 km in less than 5 days or 0.02 $m.s^{-1}$). Consequently, the 1990 dacite, which has stable hornblende phenocrysts, was stored in a deep magma reservoir prior to eruption (consistent with esti-

mated pre-eruptive pressures) and its ascent to the surface began several days before the first eruptive events.

Storage in shallow reservoirs, where conditions are outside the amphibole stability field, as well as very slow ascent of magmas, results in growth of reaction rims (Rutherford and Hill 1993). The width of the rims is positively correlated with time, and thick-rimmed phenocrysts are likely due to long shallow storage prior to eruption, whereas thin-rimmed crystals are probably induced by slow ascent from a deep storage area (Buckley et al. 2002). Magnesio-hornblende phenocrysts in hybrid andesites show thin reaction rims (10–50 μm wide), which seem to rule out a long pre-eruptive storage close to the surface.

One the other hand, solid-state amphibole and biotite dehydration, in response to influx of low-H_2O and warmer magma in the storage zone, cannot be ruled out from our petrologic study. Indeed, periodic recharges of more mafic magmas and magma mixing processes are clearly involved in the petrogenesis of the Nevado Sabancaya magmas.

Origin of magmatic enclaves

The occurrence of fine-grained magmatic enclaves has been identified as evidence for mingling of magmas of contrasting compositions and physical properties in both plutonic and volcanic igneous complexes (Eichelberger 1980; Bacon 1986; Tait 1988; Barbarin 1988; Barbarin and Didier 1991; Wiebe 1996; Murphy et al. 1998; Clynne 1999). It is generally agreed that fine-grained mafic magmatic enclaves are formed when mafic magma is trapped within a cooler silicic magma, and quenched textures are evidence of groundmass crystallization in an undercooled state (Bacon 1986). Subsequent thermal equilibration may rapidly increase the viscosity of the intruding mafic magma, preventing complete homogenisation. In general, the formation of enclaves tends to impede further mixing (Sparks and Marshall 1986). Nevertheless, mineralogical and chemical exchanges and interactions between the two magmatic components can occur extensively. Many undercooled enclaves contain reacted xenocrysts inherited from their host silicic magma, suggesting that they remained sufficiently plastic to incorporate crystals. The undercooled enclaves in Nevado Sabancaya rocks are consistent with this principle; they contain reacted xenocryts such as low-Al hornblende similar in composition to phenocrysts found in their host. However, the anorthite-rich cores of plagioclase phenocrysts ($An_{60–65}$, Fig. 4b) in the enclaves may be preserved relicts of the initial mafic magmas: their An contents suggest a basaltic andesite composition.

Bacon (1986) reviewed possible mechanisms of enclave formation. Processes commonly considered include (1) forcible injection of mafic magma, (2) mingling in a conduit, and (3) mingling across an interface layer. Magmatic enclaves within the 1990–98 lavas exhibit angular to subrounded shapes, planar contact surfaces (no crenulated margins), even-grained textures (no chilled margins) and a lack of correlation between enclave size and grain size. Neither forcible injection nor mingling in a conduit explain these textural features, which may be better explained by the disruption and dispersion of a partially crystalline interface layer (Bacon 1986; Coombs et al. 2003). Intruding turbulent fountains of hot andesitic magma lead to mixing and production of hybrid andesites, which subsequently tend to sink and accumulate at the base of the reservoir because they are denser than their host. Repeated recharges of andesitic melts may produce several hybrid layers of various physical and chemical properties. At the interface between the hybrid layers and the host magma, rapid crystallization by thermal equilibration may form partially crystalline andesitic boundary layers. Enclaves may be produced by further disruption and dispersion of these boundary layers. Mechanisms of disruption and dispersion may be either a new magma injection or the tectonic activity because they both may promote stirring at least on a local scale.

Significance of persistent vulcanian activity

The 1990–1998 eruptive activity consisted of alternating vulcanian and phreato-magmatic to phreatic events. The frequency and the intensity of the vulcanian explosions culminated during the first years (Fig. 2a). The explosions became shorter and less powerful with time, and the quiescent intervals between eruptions increased from 20–30 min (1990–1992) to 2 h or more (1994–1996). Yet, this long-lasting explosive activity has expelled only small volumes of tephra. Although moderate in size, this persistent explosive activity is difficult to reconcile with the small volumes of erupted magma. A classical model to explain vulcanian-type activity refers to gas overpressurization within the magmatic system, due to cooling and crystallization of mainly anhydrous minerals. At shallow levels, rather small amounts of crystallization are needed to produce overpressures sufficient to fracture rocks and initiate eruptions (Tait et al. 1989). Galeras volcano (Colombia) experienced a series of vulcanian eruptions between July 1992 and June 1993, following a phase of dome growth (Stix et al. 1997). At Galeras in early 1992, a decrease of degassing and a reduction of the lava dome growth were observed several months before the first vulcanian event and may be related to freezing of the magma plug within the conduit, leading to gas accumulation until rupture and eruption (Zapata et al. 1997; Stix et al. 1997). Thus low degassing rates can imply an excess of overpressure and subsequent eruption, but it can also indicate a gas-poor or degassed magma. The case of Nevado Sabancaya is different from Galeras. Satellite images have shown an open crater and no traces of a lava dome in the summit area. Furthermore, fumarolic activity since 1986 promoted regular and continuous degassing, which prevented overpressurization and bubble formation. The moderate vesicularity and the highly crystalline groundmass of the juvenile tephra suggest that increase of

magmatic pressure was not the cause of eruptions, and that magma was degassed prior to eruption. Eruptive products became less vesicular with time (Fig. 2b) suggesting that magma became more degassed. Dense blocks with radial cracks also became more abundant with time (Fig. 2b) suggesting increasing interactions between surface waters or hydrothermal fluids and the ascending magmas. Surface waters were abundant from melting of glacier ice during the first four to five years of the unrest. The area of the ice cap has decreased continuously. By 1995 the crater was 400 m across, and its surroundings were devoid of snow and ice.

The continuous occurrence of tectonic earthquakes during the course of the unrest (Antayhua et al. 2001) with hypocentres at 20 km depth or less, along N50 fractures in the Pampa Sepina area (Fig. 1b) may have promoted destabilisation of the shallow levels of the crust, thereby disrupting the magmatic system and allowing magma to rise. A survey based on satellite radar-interferometry from 1992 to 2000 (Prittchard and Simons 2002) has shown that the Pampa Sepina area also underwent surface inflation from June 1992 to April 1996, with a constant inflation rate of about 2 cm per year. The inferred depth of the deformation source was located at 11–13 km below sea level. This deformation may be related to the activity at Sabancaya, as earthquake foci and the surface deformation source are similar. Consequently, the storage and feeding systems may not be located beneath the volcano, but may be about 10 km distant.

Model for the 1990–1998 unrest

Our data show that the magma storage zone is probably located beneath the Pampa Sepina at a minimum depth of 6 km, as deduced from the amphibole stability within the dacitic magma. Unfortunately, a precise evaluation of its shape, size and location cannot be deduced from our volcanological survey and from our petrological and geochemical study alone.

Since the last eruptions in the 18th century, the magma reservoir has experienced a series of events which have contributed to the petrographical and geochemical characteristics of the erupted rocks. The main magma body consisted of dacitic magmas produced by AFC processes (Figs. 7, 8, 9). Repeated recharges of more mafic andesitic magmas intruded the base of the reservoir and induced magma mingling, mixing and hybridisation leading to the formation of hybrid magmas and hybrid crystalline interface layers.

A possible scenario of magma chamber evolution prior to and during the 1990–1998 unrest is depicted in Fig. 10. Repeated andesitic magma recharge events produced andesitic hybrid magmas, but limited convection prevented complete homogenisation resulting in small upward compositional zonation, with batches of preserved dacite in the upper part of the storage zone (Fig. 10a). A more sustained and voluminous influx of mafic andesite magma

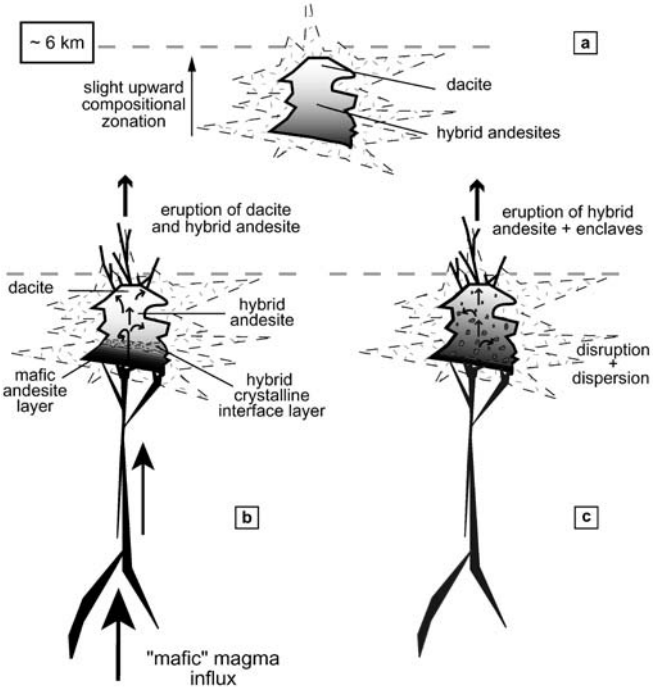

Fig. 10 Cartoon showing a possible scenario for the evolution of the magmatic system of the Nevado Sabancaya prior to and during the 1990–1998 eruptions (see explanation in text)

may have occurred from 1986–1988 leading to the reactivation of the plumbing system and enhanced heat flow (increased fumarolic activity, fracturing of the summit area and a decreasing surface area of the ice cap), and creating a hybrid crystalline boundary layer at the base of the reservoir. This caused the rise of the magma through fractures to the surface (Fig. 10b). The upper part of the reservoir containing dacitic magmas and high-Si hybrid andesites was tapped first during the first eruptions. The 1990–1992 eruptive activity was at high levels, suggesting continuous or intermittent magma flux into the reservoir, thereby feeding the eruptive column. Nevertheless, the volume of magma involved was small and the eruptive dynamics were influenced by interactions with infiltrated surface water from ice cap melting. From 1992, disruption of the hybrid foam interface layer accentuated the formation and dispersion of the mafic enclaves, allowing rise of more mafic hybrid magmas layers situated deeper in the reservoir (Fig. 10c). These magmas carried up some of the enclaves. Major seismic crises due to tectonic activity, the occurrence of magmatic enclaves and the presence of low-Si andesite lavas appeared to coincide in 1992. Further activity progressively declined in intensity, with correlative increasing occurrences of phreatomagmatic activity, suggesting the end of magma influx and a progressive return to steady-state conditions of the storage area and plumbing system.

Concluding remarks

1. The role of magma mixing in the formation of juvenile andesites erupted during the 1990–1998 eruptions is supported by mineralogical and chemical characteristics. The magma interactions and hybridisation are due to repeated recharge of mafic andesitic magmas within the magma chamber. The andesites span a narrow range of chemical composition, suggesting that complete homogenisation was not achieved.
2. In contrast, the dacite (64 wt% SiO_2), expelled during the early 1990 events, results from fractional crystallization and concomitant crustal assimilation and was preserved from the magma mixing processes. In that respect, it may approach the composition of the silicic end member of the magma mixing processes.
3. The fine-grained magmatic enclaves are evidence for mingling due to magma recharge in the magma reservoir. Their angular shapes, sharp edges and absence of grain-size decrease from core to rim support this hypothesis that they formed an interface layer, resulting from the interactions between the andesites and the more mafic recharge magmas. The composition of the recharge magmas is not known, but it may be basaltic andesite as recorded in some plagioclase phenocrysts cores found in the enclaves ($An_{60–65}$). Disruption and fragmentation of this partially crystalline layer produced the enclaves, which were dispersed within the host magma.
4. Overpressurization in the conduit was not the main cause of the explosive vulcanian-type activity, which was also influenced by interaction with surface water from the ice cap melting. The persistence of this type of intermittent regime over a long period remains problematic and poorly explained. Tectonic activity, attested by shallow tectonic earthquakes recorded during the period of unrest, may have increased the fracturing within the volcano, thereby enhancing infiltration of surface waters.
5. With respect to volcanic hazards, the low magma production rates and the declining activity after 1992 made highly explosive eruptions and pyroclastic flows unlikely. Although the amount of water from melting of the ice cap may have been large, the volumes of expelled magma were too low to produce any important mudflows, which could endanger populations living in the vicinity of the volcano.

Acknowledgements The authors thank J. Stix, J. Davidson and an anonymous reviewer for providing excellent and constructive comments. We also thank G. Wörner and B. Barbarin for suggestions and comments on early drafts of the manuscript. We are grateful to M. Veschambre for assistance on the electron microprobe, and C. Perrache and C. Bosq for invaluable help in REE and radiogenic isotopes analyses. We also thank our peruvian colleagues, O. Macedo and M. Uribe, and PhD students, A. Finizola, J. Suni and P. Navarro for their help in the field. Fundings and logistical support for this project were provided from IRD (Institut de Recherche pour le Développement), from CRV (Coordination de la Recherche Volcanologique) and from IGP (Instituto Geofisico del Peru).

References

Allègre CJ, Provost A, Jaupart C (1981) Oscillatory zoning: a pathological case of crystal growth. Nature 294:223–228

Anderson AT (1984) Probable relations between plagioclase zoning and magma dynamics, Fuego volcano, Guatemala. Am Mineral 68:125–129

Antayhua Y (2001) Analisis de la actividad sismica en la region del volcan Sabancaya y de los sismos de Maca (1991), Sepina (1992) y Cabanaconde (1998). Tesis de Licenciatura, Universidad nacional de San Agustin Arequipa, Peru, unpublished, 120 pp

Antayhua Y, Tavera H, Bernal I (2001) Analisis de la actividad sismica en la region del volcán Sabancaya (Arequipa). Bol Soc Geol Perú 92:79–88

Bacon CR (1986) Magmatic inclusions in silicic and intermediate volcanic rocks. J. Geophys Res 91(B6):6,091–6,112

Bacon CR, Hirshmann MM (1988) Mg/Mn partitioning as a test for equilibrium between coexisting Fe-Ti oxides. Am Mineral 73:57–61

Barbarin B (1988) Field evidence for successive mixing and mingling between the Piolard diorite and the Saint-Julien-la-Vêtre monzogranite (Nord Forez, Massif central, France). Can J Earth Sci 25:49–59

Barbarin B (1990) Plagioclase xenocrysts and mafic magmatic enclaves in some granitoids of the Sierra Nevada batholith, California. J Geophys Res 95(B11):17,747–17,756

Barbarin B, Didier J (1991) Macroscopic features of mafic microgranular enclaves. In: Didier J and Barbarin B (eds) Enclaves and granites. Developments in Petrology 13, Elsevier, Amsterdam Oxford New York Tokyo, pp 253–262

Buckley VJE, Sparks RSJ, Wood BJ (2002) Petrology of hornblende decompression reaction textures in the recent Soufrière Hills Volcano andesitic magma. IAVCEI meeting on explosive volcanism in subduction zones: Mount Pelée 1902–2002, abstract, pp 56

Clayton RN, Mayeda TK (1963) The use of bromine pentafluoride in the extraction of oxygen from oxides and silicates for isotopic analysis. Geochim Cosmochim Acta 27:43–52

Clynne MA (1999) A complex magma mixing origin for rocks erupted in 1915, Lassen Peak, California. J Petrol 40:105–132

Coombs ML, Eichelberger JC, Rutherford M.J (2003) Experimental and textural constraints on mafic enclave formation in volcanic rocks. J Volcanol Geotherm Res 119:125–144

Coplen TK (1993) Normalization of oxygen and hydrogen isotope data. Chem Geol 72:293–297

Davidson JP, Tepley FJ (1997) Recharge in volcanic systems: evidence from isotope profiles of phenocrysts. Science 275: 826–829

Davidson JP, De Silva SL, Holden P, Halliday AN (1990) Small-scale disequilibrium in a magmatic inclusion and its more silicic host. J Geophys Res 95:17,661–17,675

Delacour A, Paquereau P, Gerbe MC, Thouret JC, Wörner G (2002) Quaternary minor volcanic centres in southern Peru: volcanology, petrology and geochemistry. 5th International Symposium on Andean Geodynamics, Toulouse, France, abstract

De Silva SL, Francis PW (1990) Potentially active volcanoes of Peru: observations using Landsat Thematic Mapper and Space Shuttle imagery. Bull Volcanol 52(4):286–301

De Silva SL, Francis PW (1991) Volcanoes of the Central Andes. Springer, Berlin Heidelberg New York, p 216

Didier J, Barbarin B (1991) The different types of enclaves in granites — Nomenclature. In: Didier J and Barbarin B (eds) Enclaves and granites. Developments in Petrology 13, Elsevier, Amsterdam Oxford New York Tokyo, pp 19–23

Eichelberger JC (1980) Vesiculation of mafic magma during replenishment of silicic magma reservoirs. Nature 288:446–450

Gill JB (1981) Orogenic andesites and plate tectonics. Springer, Berlin Heidelberg New York, pp 1–390
Ginibre C, Kronz A, Wörner G (2002) High-resolution quantitative imaging of plagioclase composition using accumulated backscattered electron images: new constraints on oscillatory zoning. Contrib Mineral Petrol 142:436–448
Global Volcanism Network bulletin (1988) Sabancaya volcano, 13(6):10–12
Global Volcanism Network bulletin (1990) Sabancaya volcano, 15(5):2–4
Global Volcanism Network bulletin (1990) Sabancaya volcano, 15(6):2
Global Volcanism Network bulletin (1990) Sabancaya volcano, 15(7):2
Global Volcanism Network bulletin (1991) Sabancaya volcano, 16 (5):16–17
Global Volcanism Network bulletin (1991) Sabancaya volcano, 16(7):5–6
Global Volcanism Network bulletin (1991) Earthquakes, 16(7):22
Global Volcanism Network bulletin (1992) Sabancaya volcano, 17(1):8–9
Global Volcanism Network bulletin (1994) Sabancaya volcano, 19(3):8–9
Global Volcanism Network bulletin (1995) Sabancaya volcano, 20(5):4
Global Volcanism Network bulletin (1997) Sabancaya volcano, 22(7):14–15
Global Volcanism Network bulletin (1998) Sabancaya volcano, 23(8):4–5
Global Volcanism Network bulletin (2000) Sabancaya volcano, 25 (5):4
Hammarstrom JM, Zen E (1986) Aluminium in hornblende: an empirical igneous geobarometer. Am Mineralogist 71:1,297–1,313
Harmon RS, Hoefs J (1984) Oxygen isotope ratios in late Cenozoic Andean volcanics. In: Harmon RS, Barreiro BA (eds) Andean magmatism chemical and isotopic constraints, Shiva, pp 9–20
Hildreth W, Moorbath S (1988) Crustal contributions to arc magmatism in the Andes of central Chile. Contrib Mineral Petrol 98:455–489
Hollister LS, Grissom GC, Peters EK, Stowell HH, Sisson VB (1987) Confirmation of the empirical correlations of Al in hornblende with pressure of solidification of calc-alkaline plutons. Am Mineral 72:231–239
Huaman-Rodrigo D, Chorowicz J, Deffontaines B, Guillande R, Rudant JP (1993) Cadre structural et risques géologiques étudiés à l'aide de l'imagerie spatiale: la région du Colca (Andes du sud Pérou). Bull Soc géol France 164(6):807–818
James DE (1984) Quantitative models for crustal contamination in the central and northern Andes. In: Harmon RS, Barreiro BA (eds) Andean magmatism chemical and isotopic constraints, Shiva, pp 124–138
Johnson MC, Rutherford MJ (1989) Experimental calibration of aluminium-in-hornblende geobarometer with application to Long Valley caldera (California) volcanic rocks. Geology 17:837–841
Juvigné E, Thouret J-C, Gilot E, Leclercq L, Gourgaud A (1998) L'activité du volcan Nevado Sabancaya (Pérou) au cours de l'Holocene. Quaternary 9(1):45–51
Kanokea I, Guevara C (1984) K-Ar age determinations of late Tertiary and Quaternary volcanic rocks, Southern Peru. Geochemical Journal 18:233–239
Kink BA, Ellison RA, Hawkins MP (1986) The geology of the Cordillera occidental and Altiplano West of lake Titicaca, southern Peru. British Geol Surv Open-File Report 353 pp
Koyaguchi T (1986) Textural and compositional evidence for magma mixing and its mechanism, Abu volcano group, southwestern Japan. Contrib Mineral Petrol 93:33–45
Leake BE, Woolley AR, Arps CES, Birch WD, Gilbert MC, Grice JD, Hawthorne FC, Kato A, Kisch HJ, Krivovichev VG, Linthout K, Laird J, Mandarino JA, Maresch WV, Nickel EH, Rock NMS, Schumacher JC, Smith DC, Stephenson NCN, Ungaretti L, Whittaker EJW, Youzhi G (1997) Nomenclature of amphiboles: Report of the Subcommittee on Amphiboles of the International Mineralogical Association, Commission on new minerals and mineral names. Am Mineral 82:1,019–1,037
Lofgren GE (1974) An experimental study of plagioclase crystal morphology: isothermal crystalllization. Am J Sci 274:243–273
Lofgren GE (1980) Experimental studies on the dynamic crystallization of silicate melts. In Hargraves RB (ed), Physics of magmatic processes, Pinceton Univ Press Princeton NJ, pp 487–551
Mégard F (1987) Cordilleran Andes and marginal Andes: a review of Andean geology north of the Arica elbow. American Geophys Union, Geodynamics series, vol. 18, Washington, pp 71–95
Mering C, Huaman-Rodrigo D, Chorowicz J, Deffontaines B, Guillande R (1996) New data on the geodynamics of southern Peru from computerized analysis of SPOT and SAR ERS-1 images. Tectonophysics 259:153–169
Morimoto N, Fabries J, Fergusson AK, Ginzburg IV, Ross M, Seifert FA, Zussman J, Aoki K, Gottardi G (1988) Nomenclature of pyroxenes. Bull Mineral 111:535–550
Murphy MD, Sparks RSJ, Barclay J, Caroll MR, Lejeune AM, Brewer TS, Macdonald R, Black S, Young S (1998) The role of magma mixing in triggering the current eruption at the Soufrière Hill volcano, Monserrat, West Indies. Geophys Res Lett 25:3,433–3,436
Nakamura M, Shimakita S (1996) Partial dissolution kinetics of plagioclase: implication for magma mixing time scale and origin of melt inclusion. EOS 77:F841
Nakamura M, Shimakita S (1998) Dissolution origin and syn-entrapment compositional changes of melt inclusions in plagioclase. Earth Planet Sci Lett 161:119–133
Palacios M (1995) Geologia del Peru. Estratigrafia. Carta Geologia Nacional, INGEMMET, Lima, Bolt. 55:45–86
Pearce TH (1994) Recent work on oscillatory zoning in plagioclase. In: Parson I (ed) Feldspars and their reactions. Kluwer, Dordrecht, pp 313–349
Pin C, Briot D, Bassin C, Poitrasson F (1994) Concomitant separation of strontium and samarium-neodynium for isotopic analysis in silicate samples, based on specific extraction chromatography. Anal Chim Acta 298:209–217
Pin C, Santos Zalduegui J F (1997) Sequential separation of light rare-earth elements, thorium and uranium by miniaturized extraction chromatography: application to isotopic analyses of silicate rocks. Anal Chim Acta 339:79–89
Prittchard ME, Simons M (2002) A satellite geodetic survey of large-scale deformation of volcanic centres in the central Andes. Nature 418:167–171
Rutherford MJ, Devine JD (1988) The May 18, 1980, eruption of Mount St Helens, 3, Stability and chemistry of amphibole in the magma chamber. J Geophys Res 93:11,949–11,959
Rutherford MJ, Hill PM (1993) Magma ascent rates from amphibole breakdown: an experimental study applied to the 1980–1986 Mount St Helens eruptions. J Geophys Res 98(B11): 19,667–19,685
Schmidt MW (1992) Amphibole composition in tonalite as a function of pressure: an experimental calibration of the Al-in-hornblende barometer. Contrib Mineral Petrol 48:211–227
Seaman SJ (2000) Crystal clusters, feldspar glomerocrysts, and magma envelopes in the Atascosa Lookout lava flow, southern Arizona, USA: recorders of magmatic events. J Petrol 41(5):693–716
Sébrier M, Soler P (1991) Tectonics and magmatism in the Peruvian Andes from late Oligocene time to present. In: Harmon RS, Rapela CW (eds) Andean magmatism and its tectonic setting, Geol Soc Amer Spec Paper 265, pp 259–278
Sébrier M, Lavenu A, Fornari M, Soulas JP (1988) Tectonics and uplift in Central Andes (Peru, Bolivia and Northern Chile) from Eocene to present. Géodynamique 3(1–2):85–106
Sébrier M, Mercier JL, Mégard F, Laubacher G, Carey-Gaihardis E (1985) Quaternary normal and reverse faulting and the state of stress in central Andes of southern Peru. Tectonics 4:739–780

Singer B, Dungan MA Layne GD (1995) Textures and Sr, Ba, Mg, Fe, K, and Ti compositional profiles in volcanic plagioclase: clues to the dynamics of calc-alkaline magma chambers. Am Mineral 80:776–798

Soler P (1990) Relation of magmatic activity to plate dynamics in central Peru from late Cretaceous to present. In: Kay SM, Rapela CW (eds) Plutonism from Antarctica to Alaska, Geol Soc Amer Spec Paper 241, pp 173–192

Sparks RSJ, Marshall LA (1986) Thermal and mechanical constraints on mixing between mafic and silicic magmas. J Volcanol Geotherm Res 29:99–124

Sparks RSJ, Sigurdsson H, Wilson L (1977) Magma mixing: a mechanism for triggering acid explosive eruptions. Nature 267:315–318

Spencer KJ, Lindsley DH (1981) A solution model for coexisting iron-titanium oxides. Am Mineral 66:1189–1201

Stix J, Torres C R, Narvaez M L, Cortés J GP, Raigosa A J, Gomez M D, Castonguay R (1997) A model of vulcanian eruptions at Galeras volcano, Colombia. J Volcanol Geotherm Res 77:285–303

Tait SR (1988) Samples from the crystallizing boundary layer of a zoned magma chamber. Contrib Mineral Petrol 100:470–483

Tait SR, Jaupart C, Vergniolle S (1989) Pressure, gas content and eruption periodicity of a shallow, crystallizing magma chamber. Earth Planet Sci Lett 92:107–123

Tepley III FJ, Davidson JP, Clynne MA (1999) Magmatic interactions as recorded in plagioclase phenocrysts of Chaos Crags, Lassen Volcanic Center, California. J Petrol 40:787–806

Thouret J-C, Guillande R, Huaman D, Gourgaud A, Salas G, Chorowicz J (1994) L'activité actuelle du Nevado Sabancaya (Sud Pérou): reconnaissance géologique et satellitaire, évaluation et cartographie des menaces volcaniques. Bull Soc géol France 165(1):49–63

Thouret J-C, Juvigné E, Loutsch I, Chavez Chavez JA (2001) Historic volcanic activity and human sacrifices by the Incas in Southern Peru. In: Juvigné E, Raynal J-P (eds) Tephras: chronology, archaeology. Dossiers de l4Archéo-Logis, pp 219–226

Tsuchiyama A (1985) Dissolution kinetics of plagioclase in the melt of the system diopside-albite-anorthite, and origin of dusty plagioclase in andesites. Contrib Mineral Petrol 89:1–16

Vennemann TW, Smith HS (1990) The rate and temperature of reaction of ClF3 with silicate minerals, and their relevance to oxygen isotope analysis. Chem Geol (Isotope Geosciences Section) 86:83–88

Wiebe RA (1996) Mafic-silicic layered intrusions: role of basaltic injections on magmatic processes and evolution of silicic magma chambers. Trans Royal Soc Edinburgh, Earth Sci 87:233–242

Zapata G JA, Calvache V ML, Cortés J GP, Fisher TP, Garzon V G, Gomez M D, Narvaez M L, Ordoñez V M, Ortega E A, Stix J, Torres C R, Williams SN (1997) SO2 fluxes from Galeras volcano, Colombia, 1989–1995: Progressive degassing and conduit obstruction of a Decade Volcano. J Volcanol Geotherm Res 77:195–208